– For internal NASA use only –

Lunar Impact Ejecta Benchmark and Models

Anthony M. DeStefano
NASA, MSFC, EV44

January 27, 2021

Contents

1 Executive Summary **1**

2 MEM3 Based Lunar Ejecta Modeling **1**
2.1 Assumptions and Simplifications 2
2.2 Algorithm 3
2.3 Near-Earth Object Environment 4
2.3.1 Kinetic-Energy-Limited Flux 4
2.3.2 Mass-Limited Flux 5
2.3.3 Speed Distribution 5
2.4 Latitudinal Dependence of Primary (sporadic meteoroids) Flux 6
2.5 Regolith Size Distribution 7
2.5.1 Weighted by number and not mass 9
2.6 Ejected Mass from an Impactor 11
2.7 Ejecta Mass Distribution Function 12
2.7.1 Zenith Distribution Function 12
2.7.2 Azimuth Distribution Function 17
2.7.3 Speed Distribution Function 19
2.7.4 Speed Bin Centers 20
2.7.5 Normalization Term 20
2.8 Meteoroid Projectile Mass Distribution 21
2.9 Meteoroid Projectile Density Distribution 23
2.10 Meteoroid Projectile Speed and Angle Distribution 23
2.11 Secondary Ejecta Distance, Speed, & Angle 23
2.11.1 Coriolis Force 28
2.12 Distance and Bearing 28

3 NASA SP-8013 Meteoroid Environment Model - 1969 **29**
3.1 Comparison of Scaling Laws of New and Old Ejecta Models 31

4 Analytic Study of Secondary Lunar Ejecta **32**
4.1 Total Ejected Mass 32
4.2 Estimated Secondary Ejecta at a ROI with Normally Impacting Primaries 33
4.2.1 Isotropic Azimuth and $45°$ Zenith Distributions 35
4.2.2 Isotropic Azimuth and Zenith Distributions 35
4.3 Secondary Ejecta at a ROI vs. Distance 39
4.4 Secondary Ejecta at a ROI vs. Speed and Distance 40
4.5 Secondary Ejecta at a Satellite of the Moon 43

References **46**

List of Figures

1 Mass-limited speed distribution at the lunar surface. 5
2 Fluxes (as a function of impact speed and angle from the horizon) of the low density population (a) and (b), and the high density population (c) and (d) impacting the Moon at the equator (a) and (c), and the north/south pole (b) and (d). 6
3 Geotechnical particle size distribution: middle curve showing the average distribution; left-hand and right-hand curves showing ± 1 standard deviation [*Carrier III*, 2003]. Note, that the percent passing is normalized by mass and not particle number [see *Carrier*, 1973]. 7
4 Non-linear fit of Figure 3 (the average distribution) with Eq. 2.7 in SciDAVis, giving the constants for a, b, c, and d. 9
5 Non-linear fit of Table 1 with Eq. 2.15 in SciDAVis, giving the constants for A, a, b, and d. 10
6 For larger impact angles that are more grazing to the surface, the zenith and azimuth ejecta distributions become asymmetric. Starting at $70°$, the peak ejecta angle α_{max} becomes negative in an exclusion range, as shown in the figure. This means that the $-\alpha_{max} \to \alpha_{max}$ and $\beta - \beta_i \to \beta - \beta_i + \pi$. In this model, for impact angles near $90°$, most of the ejecta is concentrated in the downstream direction. 14
7 The Grün interplanetary meteoroid flux as a function of limiting particle mass [*Moorhead et al.*, 2019, Figure 1]. 22
8 Non-linear fit of Figure 7 with Eq. 2.92 in SciDAVis, giving the constants for a, b, c, and d. 22
9 Meteoroid density distribution according to the MEM3 User Guide. The apex and toroidal meteoroid sources constitute the low-density population, while the helion/antihelion source constitutes the high-density population. Each set of densities follows a log-normal distribution [c.f. Figure 11, *Moorhead et al.*, 2019]. 24
10 Non-linear fit of the low density profile in Figure 9 with Eq. 2.95 in SciDAVis, giving the constants for $a \to A$, $s \to \sigma$, and $m \to \mu_\delta$. 24
11 Non-linear fit of the high density profile in Figure 9 with Eq. 2.95 in SciDAVis, giving the constants for $a \to A$, $s \to \sigma$, and $m \to \mu_\delta$. 25

12 The color gradient shows the distance a projectile goes with a given ejected speed and zenith angle. The cyan dashed line gives the optimal angle for a given speed to reach the furthest distance, i.e., Eq. (2.114). The red dashed line shows for which pairs of speeds and zenith angles are required to hit the antipodal point. As an example, all ejecta with speed and angle pairs between the two black curves will reach a location between 0.05 and 0.06 lunar circumference units away, using Eq. (2.110). 26
13 Average cumularive lunar ejecta flux-mass distribution for each of three ejecta velocity intervals [*Cour-Palais*, 1969]. 30
14 The geometrical term of the secondary ejecta speed distribution $\mathcal{G}(D, v)$ as a function of speed for various distances in units of lunar radii r_m. . . . 42
15 The geometrical term of the secondary ejecta distance distribution $\mathcal{G}(D, v)$ as a function of distance, in units of lunar radii r_m, for various speeds in units of escape velocity v_{esc}. 42

List of Tables

1 Digitized data points from Figure 3, see *Carrier III* [2003]. 8
2 Cone angles of upstream and downstream of impact derived from Figure 18 of *Gault and Wedekind* [1978]. 14

1 Executive Summary

The goal of the secondary ejecta model discussed in this report is to provide an updated environment to replace the Apollo-era model given in *Cour-Palais* [1969]. This update will be published in the next revision (rev. I) of the SLS-SPEC 159 Design Specification for Natural Environments (DSNE). Our primary customer of this update will be the Human Landing System (HLS) Appendix H contractors who will be designing an integrated human landing system to land near the Moon's south pole by 2024, in addition to contractors building longer-term and more sustainable solutions for the 2026+ time frame. The DSNE is a required document for HLS Appendix H contractors that provides terrestrial, in-space, and lunar natural environment definitions.

The secondary ejecta environment will be the mass-limited particle flux as a function of both altitude and azimuth angles as well as speed for various latitudinal locations on the Moon. This environment will feed into bumper codes that compute risk of penetration by the secondary ejecta to different materials. Currently, bumper codes can ingest output from the Meteoroid Environment Model, so we chose to follow the same output format to help facilitate ease-of-use by these bumper codes. It is known that the net secondary ejecta flux is much greater than the net primary flux, however at very different speed (much lower) and angular distributions. At lower speeds, the physics of penetration due to the ejecta is much different than the high-speed primary ejecta. Therefore, it is important to quantify these effects in order to hone in on the risk involved.

Our primary goal with this new secondary ejecta model encompasses the need to include information about impact angles (including azimuth) as well as the ejecta field angular distribution. Empirical decisions were based on or aided by experiments given in the literature, so we included as much information as necessary to incorporate leading order characteristics in a qualitative way. We did this in light of producing an engineering solution of computing secondary fluxes on the Moon from impact sizes that range from 10^{-6} g to $\sim 10^{15}$ g.

2 MEM3 Based Lunar Ejecta Modeling

The Meteoroid Engineering Model (MEM) describes the sporadic meteoroid complex, or the background meteoroid environment, and does not include meteor showers. The impactor masses range from $1\ \mu$g to 10 g. Larger impactor masses must be dealt with differently [e.g., see *Neukum et al.*, 2001; *Brown et al.*, 2002]. We use output from MEM in order to estimate the number of particles per area per year greater than a certain mass (or the particle flux mass spectrum) due to secondary ejecta from meteoroid impacts on the Moon. The risk due to impacts on the Moon is driven by secondary ejecta and not the primary meteoroid flux.

We begin by first describing the algorithm at which we plan to use to compute the particle flux mass spectrum at a given point on the Moon. In essence, the algorithm is based on the reverse Monte-Carlo idea. We then go into detail about how to compute each step of the algorithm, either borrowing from the literature or making our own derivations.

2.1 Assumptions and Simplifications

There are several assumptions and simplications made in our model in order to provide traceable engineering solutions. We provide a list below with the most important assumptions in no particular order and provide comments on each.

1. The ejecta particle distribution is the same as the virgin regolith particle distribution.

    - Crater sizes that are less than ~ 50 m will mostly sample the top-most layer of regolith. For impactors that generate larger craters, such as those found in the NEO population, this assumption breaks down. We expect the very large craters (> 100 m) to introduce larger bolder sizes not present in the virgin regolith particle distribution. We believe these large bolders to be in the far tail of the distribution function and are very unlikely. Ignoring the large particle population will inflate the smaller particle sizes, which may help to offset the error in the risk, but this offset is not for certain.

2. The scaling law provided by *Housen and Holsapple* [2011] is valid for all impactors simulated in our model.

    - Both authors are experts in the field of high-velocity impacts and have done much work to develop scaling laws that are valid for several orders of magnitude of impact sizes. For extremely small size impacts, such as impactor masses near 10^{-6} g, the scaling laws might not be valid since this is roughly the 50-percentile size of the regolith particle size distribution. For simplification, we ignore this issue for now.

3. The azimuth and zenith angle distribution functions are given empirically and do not depend on the size of impact or speed of impact, only the angle of impact.

    - The azimuth distribution function follows published work done by ESA contract work [*Miller*, 2017]. We modified the azimuth distribution function at highly oblique angles to include information about ejecta patterns that exhibit the so called butterfly pattern [*Shuvalov*, 2011]. Depending on the latitude of the impact location, there can be a substantial component of the flux that can come into play.
    - The zenith angle distribution does have an azimuthal and impact angle dependence that follows fits from *Gault and Wedekind* [1978]. When the outgoing zenith angle tips over (when it goes negative), we ignore this component as an exclusion zone and implicitly include the fluxes in the downstream direction. This avoids having to deal with multi-valued functions which would require special cases to handle.
    - Since the integration is complicated enough, we do not want to complicate things by introducing a velocity dependence in the angle distributions. We know this to be the case in reality, but we ignore this dependence for simplicity.

4. The regolith density is constant over the whole Moon and for all depths.
    - The regolith density differs from highlands to mare in addition to depth. However, building a density map of the Moon is beyond the scope of this engineering model. We also note that the density dependence is raised to a small power (~ 0.2), so this will have a minor effect on total mass ejected from the crater. On the other hand, density can have a great impact on ballistic equations and bumper computations.
5. The Moon is a perfect sphere with a mono-polar gravity well (i.e., we ignore irregularities in the lunar surface and gravity).
    - We expect landing locations to not be deep in craters, which can be hazardous to con-ops. Local terrain can have a shadowing effect, so our calculations could be seen as a worst-case in this sense since we ignore these.
    - Most of the ejecta will have relatively short transit times and therefore will only be slightly perturbed by the irregular gravity well of the Moon. We also ignore Coriolis forces, which can be shown to be insignificant on the Moon for all relevant ejecta speeds.
6. The angular distribution of NEA's on the lunar surface are modeled after the high density population provided by MEM.
    - Roughly speaking, the NEA's we consider are in the ecliptic plane, as is the high density population of sporadic meteors in MEM. The speed distributions do differ so we re-scale the angular distribution from MEM using the NEA speed distribution.

2.2 Algorithm

1. For a given location on the Moon, compute the particle flux mass spectrum
2. For each source location
    - Defines the distance D from the source required to compute the ejecta velocity $v = v(D, \gamma)$.
3. For each ejecta angle γ
    - Completely defines the ejecta velocity $v = v(D, \gamma)$
4. For each meteoroid impact angle α (from MEM output)
    - At the moment, we will sum over the azimuthal angle and assume isotropic azimuthal seconday ejecta (this is not the case for impact angles less than 30° from the horizon).
5. For each meteoroid impact speed U
6. For each impactor density δ

- We only need to compute this once for each target material, and can factor out as a constant. The density is given as an output in MEM.

7. For each impactor mass m_p

   - We can integrate this out. At first glance, we will get a list of hypergeometric functions, but we only need to evaluate these once and factor out as a constant. The mass distribution is given in MEM Eq. (2.1).

8. For each ejecta particle size m_e

   - We can integrate the particle size distribution, but we will need to keep track of each mass size m_e.

2.3 Near-Earth Object Environment

The near-Earth object (NEO) environment introduces mass sizes of impactors beyond 10 g, outside of MEM's size range. Unlike MEM, the NEO's consist of small asteroids and comets between 0.1 and 1000 m in diameter. The work outlined in this section originates from analysis done by Althea Moorhead (see Memo OSMA/MEO/Lunar-001). The goal of the this analysis converts energy-limited fluxes of NEO's at the Earth to mass-limited fluxes at the Moon using *Brown et al.* [2002] as a starting point.

2.3.1 Kinetic-Energy-Limited Flux

Brown et al. [2002] use a combination of bright bolide data, infrared and acoustic data, satellite observations, and telescopic observations of small asteroids to construct a power law describing the cumulative flux of large objects onto Earth, given by

$$\log_{10} N = a - b \log_{10} \mathrm{KE}, \tag{2.1}$$

where KE is the kinetic energy of the impactor in kilotons TNT equivalent (4.184×10^{12} J), N is the number of objects impacting the Earth per year with a given kinetic energy or greater, and the constants are $a = 0.5677$ and $b = 0.9$.

We convert this flux to MKS units by assuming the Earth has an effective radius of 6471 km (including 100 km of atmosphere capable of ablating meteoroids). The resulting kinetic-energy-limited flux per square meter per year is given by

$$f_{\oplus}(\mathrm{KE}) = 7.023 \times 10^{-15} \mathrm{KE}^{-0.9}. \tag{2.2}$$

To obtain Equation (2.2), we have divided by the surface are of the Earth. Thus, $f_{\oplus}$ reports the flux per unit surface area. One can convert Equation (2.2) to a flux per cross-sectional are, if desired, by multiplying by 4. Note that the bulk density is assumed to be 3000 kg m^{-3} [*Brown et al.*, 2002].

2.3.2 Mass-Limited Flux

The mass-limited flux at the lunar surface can be shown to be

$$g_{☾}(m) = 2.89 \times 10^{-11}\text{m}^{-2}\text{yr}^{-1} \cdot m^{-0.9}, \tag{2.3}$$

where m is the mass of the impactor in kg.

When converting the NEO flux into secondary flux using Equation (2.18), we must integrate the flux per mass with m

$$G_{☾m} = \int_{m_{min}}^{m_{max}} dm \frac{-dg_{☾}(m)}{dm} m, \tag{2.4}$$

where

$$\frac{dg_{☾}(m)}{dm} = -2.601 \times 10^{-11}\text{m}^{-2}\text{yr}^{-1} \cdot m^{-1.9}. \tag{2.5}$$

Therefore, using $m_{min} = 10$ g (extrapolating down to the upper-limit of MEM) and $m_{max} = 1.57 \times 10^{15}$ g (mass of a sphere taking 1000 m as the diameter and 3000 kg m^{-3} as the density), Equation (2.3) becomes

$$G_{☾m} = 4.148 \times 10^{-9}\text{m}^{-2}\text{yr}^{-1} \cdot \text{kg}, \tag{2.6}$$

which represents the mass flux in the given range above.

2.3.3 Speed Distribution

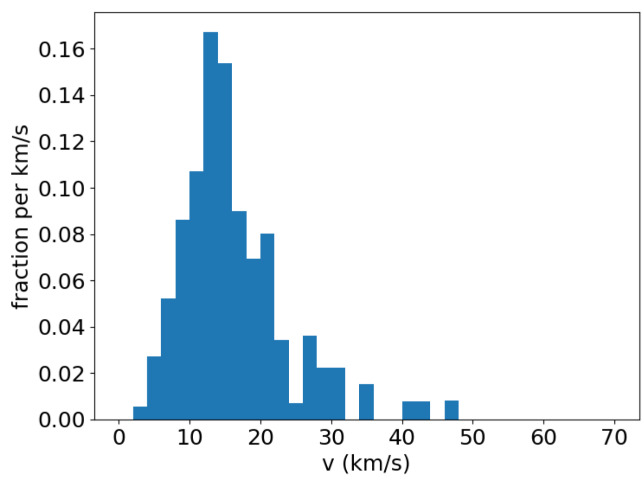

Figure 1: Mass-limited speed distribution at the lunar surface.

The speed distribution of NEO's is shown in Figure 1. The values (fraction of flux per bin) in each bin are midpoint values, where the bins have a size of 2 km s^{-1}. Note also that because the flux is a power law, this speed distribution is independent of limiting mass.

2.4 Latitudinal Dependence of Primary (sporadic meteoroids) Flux

The primary flux of sporadic meteoroids onto the surface of the Moon changes depending on the latitudinal location on the Moon. Because of this effect, we generated ephemeris data[1] for different latitudes on the Moon in 5-degree increments from pole to pole along the meridian. We chose a time frame of 19 years, or a Metonic cycle, which takes into account many different Sun-Earth-Moon geometries in order to provide a time/longitude-averaged primary flux environment.

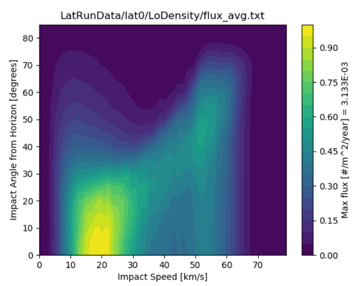

(a) Low density population impacting at the equator.

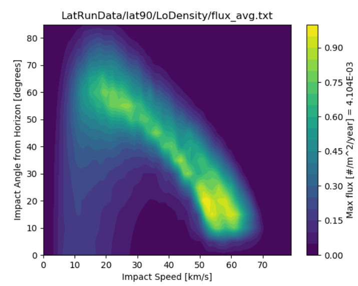

(b) Low density population impacting at the north pole.

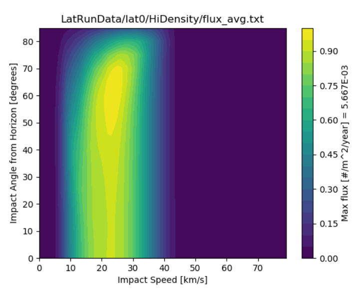

(c) High density population impacting at the equator.

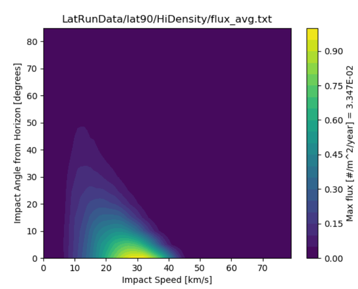

(d) High density population impacting at the north pole.

Figure 2: Fluxes (as a function of impact speed and angle from the horizon) of the low density population (a) and (b), and the high density population (c) and (d) impacting the Moon at the equator (a) and (c), and the north/south pole (b) and (d).

As an example, in Figure 2, we show the speed-angle flux distribution at the equator and poles for the low and high density MEM populations. Note that the fluxes in the northern and southern hemispheres are symmetric about the equator. We can see from Figure 2 that the impact angles and speeds are highly dependent on the impact latitude on the Moon and hence warrant a more sophisticated approach to computing the secondary fluxes. We cannot assume that most impacts are at 45 degrees or are not highly oblique. How this latitude dependence affects the secondary flux is not

[1] Horizons Ephemeris System <horizons@ssd.jpl.nasa.gov>.

entirely clear, except for the fact that we hypothesize that the secondary fluxes will be themselves dependent on latitude.

2.5 Regolith Size Distribution

For relatively small impact sizes (craters $< 30 - 50$ m), we can generally assume the secondary ejecta follows that of the original regolith. The cumulative distribution function (CDF) of the particle sizes can be fit to many observations, as shown in Figure 3.

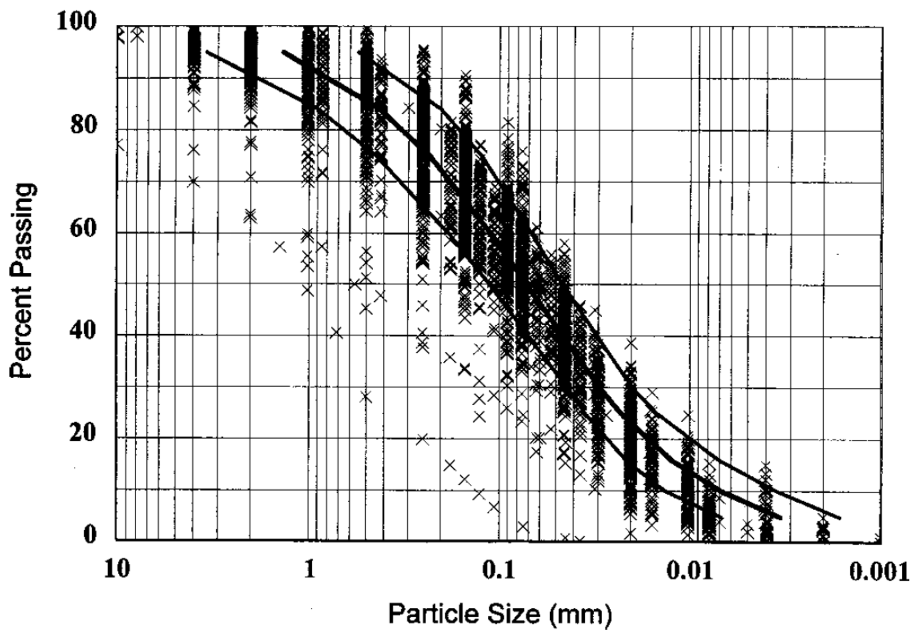

Figure 3: Geotechnical particle size distribution: middle curve showing the average distribution; left-hand and right-hand curves showing ± 1 standard deviation [*Carrier III*, 2003]. Note, that the percent passing is normalized by mass and not particle number [see *Carrier*, 1973].

The digitized data from Figure 3 is shown in Table 1.

In order to parameterize the CDF from Figure 3, we make a fit to the model equation

$$C_{\text{Moon}} = 1 - \exp\left(\frac{-1}{ax^b + cx^d}\right), \tag{2.7}$$

which is an exponential distribution with two scales defined by a and c, with x in units of mm. In SciDAVis, we make the fit with the x-axis on a logarithmic scale to give equal weight to both small and large scaled particles. The results for the curve fit are shown

Table 1: Digitized data points from Figure 3, see *Carrier III* [2003].

Particle Diameter (mm)	Cumulative Percent by Mass
0.003380248352585	5.17682028091534
0.003794441295246	6.09401642297017
0.00451292465605	7.2776812909626
0.0053674729594	8.4354410787182
0.006383732464611	9.71063723021409
0.007592176031253	11.2086170717467
0.009029116435596	12.9190185712213
0.010737989052827	14.65100763756
0.012769865152208	16.6247774527757
0.015185144104918	19.116648872728
0.018057261192048	21.6025237463292
0.02136872870221	24.2948870610798
0.025044648784976	27.0334149904509
0.029494364580794	29.8741284657866
0.033098954040892	32.8807708128992
0.037145453042138	35.6150479687852
0.042499223173782	38.2089250804786
0.048155933590968	41.1181012805662
0.054042887826956	43.8970091889745
0.060942690951498	46.6685810695819
0.068720899309714	49.7075873197331
0.077869796000019	52.4248808897808
0.087812953450079	55.0874612212659
0.098550426314892	57.6779504306929
0.112206724061769	60.6265864834011
0.127759476997186	63.3415731364729
0.145465039759366	66.2037864789212
0.168035843630453	69.131911259623
0.19411176280305	71.9484525505802
0.222083419318477	74.7285290349147
0.259044020108005	77.2129935126797
0.30803890584547	79.7150699642405
0.366294873918129	82.3305792671413
0.435590409221425	84.5720349114709
0.518029785192508	86.3256115446736
0.616085725364177	87.9108051563369
0.732705596850257	89.4631856663669
0.871382022892136	91.1718601604924
1.03629488039837	92.9535006306183
1.23245384670266	94.5235829454768

in Figure 4. We found that a simple exponential distribution with a single scale was insufficient, hence the reason we opted for a two-scaled exponential distribution.

```
[12/30/2019 5:40:09 PM          Plot: "Graph2"]
Non-linear fit of dataset: Table2_2, using function: 100*(1-exp(-1/(a*(10^x)^b+c*(10^x)^d)))
Y standard errors: Unknown
Nelder-Mead Simplex algorithm with tolerance = 0.0001
From x = -2.482108151 to x = 0.134259956
a  = 0.0548044684398436 +/- 0.00569348851446585
b  = -1.01472478485333 +/- 0.0196858460040614
c  = 0.337499285612252 +/- 0.0049924392579481
d  = -0.251808155531636 +/- 0.0188844274561765
---------------------------------------------------------------------------------
Chi^2 = 8.25978651917647
R^2 = 0.999849854428033
---------------------------------------------------------------------------------
Iterations = 89
Status = success
---------------------------------------------------------------------------------
```

Figure 4: Non-linear fit of Figure 3 (the average distribution) with Eq. 2.7 in SciDAVis, giving the constants for a, b, c, and d.

To compute the probability distribution function (PDF), we can simply take the derivative of the CDF with respect to x, which results in the following equation:

$$P_{\text{Moon}} = -A\frac{abx^{b-1} + cdx^{d-1}}{(ax^b + cx^d)^2} \exp\left(\frac{-1}{ax^b + cx^d}\right), \tag{2.8}$$

where A is the normalization constant. In theory, this should be equal to 1, but since we are not taking our particle size from 0 to infinity, we need to compute the value of A. If we assume the particle size can range from 0.001 mm to 10 mm, then $A = 1.02218$.

2.5.1 Weighted by number and not mass

In order to compare with NASA SP-8013 [*Cour-Palais*, 1969], we first must convert the distribution function normalized by number and not mass. We can then write

$$N_{ej}(x) \sim \int_x^\infty \frac{dx}{m(x)} \frac{d(C_{\text{Moon}}(x))}{dx}, \tag{2.9}$$

where x is the particle diameter, and

$$m(x) = \frac{\pi}{6}\rho x^3. \tag{2.10}$$

Instead of fitting C_{Moon} to Figure 3 directly, we will approximate using a power-law interpolation technique such that

$$C_{\text{Moon}}(x) = y_i \left(\frac{x}{x_i}\right)^{b_i}, \tag{2.11}$$

where

$$b_i = \frac{\log(y_{i+1}/y_i)}{\log(x_{i+1}/x_i)}, \tag{2.12}$$

and where $x_i \leqslant x \leqslant x_{i+1}$, for data x_i from Figure 3 (also shown in Table 1). Therefore, we can write Equation (2.9) as

$$N_{ej}(x) \sim \frac{6}{\pi\rho}\frac{b_i}{3-b_i}\frac{y_i}{x_i^{b_i}}x^{b_i-3}. \tag{2.13}$$

If we want to normalize Equation (2.13) to unity for a certain size x_{norm}, we then have

$$N_{ej}(x) = \frac{b_i(3-b_n)}{b_n(3-b_i)}\frac{x_n^{b_n}}{x_i^{b_i}}\frac{y_i}{y_n}\frac{x^{b_i-3}}{x_{\text{norm}}^{b_n-3}}, \tag{2.14}$$

where $x_n \leqslant x_{\text{norm}} \leqslant x_{n+1}$.

If we apply the method of Equation (2.14) to the Carrier 2003 data shown in Table 1 and make a fit using a double power-law expression given by

$$N_{ej}(x) = \frac{A}{\left(\frac{x}{a}\right)^b + x^d}, \tag{2.15}$$

then the fit parameters can be computed as shown in Figure 5.

```
[9/23/2020 4:38 PM          Plot: "Graph2"]
Non-linear fit of dataset: Table2_2, using function: log10( A/( (10^x/a)^b + (10^x)^d) )
Y standard errors: Unknown
Scaled Levenberg-Marquardt algorithm with tolerance = 0.0001
From x = -2.47105139019728 to x = 0.090770664665162
A  = 0.00921624902003821 +/- 0.0046037913480369
a  = 0.346681782684812 +/- 0.0532546027488427
b  = 3.60486296421154 +/- 0.0789704288933391
d  = 2.32993070045899 +/- 0.096749147779981
---------------------------------------------------------------------------------------
Chi^2 = 0.172121195592017
R^2 = 0.999116143889293
---------------------------------------------------------------------------------------
Iterations = 0
Status = success
---------------------------------------------------------------------------------------
```

Figure 5: Non-linear fit of Table 1 with Eq. 2.15 in SciDAVis, giving the constants for A, a, b, and d.

We can also include even smaller particles (dust) of the lunar regolith distribution from LADEE measurements and modeling [*Horányi et al.*, 2015]. They showed that the LDEX measurements indicate the ejected particles follow a power law $m^{-\alpha}$, where $\alpha \approx 0.9$, for the range of particle sizes between 0.1 μm and 5 μm [*Horányi et al.*, 2014]. This implies a relation of $x^{-2.7}$, where x is the particle diameter, since $m \sim x^3$. If we extend the cumulative number distribution by size $N_{ej}(x)$ from Equation (2.15), we have a triple power-law distribution

$$N_{ej}(x) = \frac{A}{\left(\frac{x}{a}\right)^b + \frac{1}{x^{-d} + \left(\frac{x}{c}\right)^{-f}}}, \tag{2.16}$$

where

$$\begin{aligned} A &= 9.659 \times 10^{-3} \text{ number of particles} > x \\ a &= 0.34668 \text{ mm}, \\ b &= 3.69, \\ c &= 0.4326 \text{ mm}, \\ d &= 2.05, \\ f &= 2.7. \end{aligned} \tag{2.17}$$

Since the scales a and c are of the same order, the index d is dominated by the overlap region, which really acts like $(d + f)/2 = 2.375$ and is comparable to the low end of the Carrier model in Equation (2.15) for an index of 2.33.

2.6 Ejected Mass from an Impactor

From *Housen and Holsapple* [2011], we can compute the mass ejected faster than v in terms of impactor properties, given by

$$M(v; \rho; m, \delta, U, \alpha) = M(> v) = C_4 m \left[\frac{v}{U\Theta(\alpha)} \left(\frac{\rho}{\delta}\right)^{\frac{3\nu-1}{3\mu}}\right]^{-3\mu}, \tag{2.18}$$

where

- v: secondary ejecta speed,
- ρ: target density,
- m: projectile mass,
- δ: projectile density,
- U: projectile speed,
- α: projectile impact angle (from horizon),

and

$$C_4 = \frac{3k}{4\pi} C_1^{3\mu}, \tag{2.19}$$

where the constants k, C_1, ν, and μ depend on the specific material properties, see Table 3 of *Housen and Holsapple* [2011]. The impact angle modification equation $\Theta(\alpha)$ can be chosen to be

$$\Theta(\alpha) = \begin{cases} 1 \\ \sin\alpha \\ \sin(\sqrt{\alpha_0^2 + \alpha^2}), \ \alpha_0 \sim 5° - 15°. \end{cases} \tag{2.20}$$

For the ejected mass that is in a given velocity range, we can define $\Delta M(v_2, v_1)$ as

$$\Delta M(v_2, v_1) = M(> v_2) - M(> v_1). \tag{2.21}$$

2.7 Ejecta Mass Distribution Function

The mass ejected from the crater, $M(> v)$, from Eq. (2.18), is the total mass ejected from an impact at velocities greater than v. However, we would like to know how this ejecta is distributed in speed and solid angle so we can map the ejecta to a particular surface location on the Moon. We can then set Eq. (2.18) in terms of the integral over the distribution functions of speed and solid angle as

$$M(> v) = \int_v^\infty \int_0^{2\pi} \int_0^{\pi/2} \sin\alpha d\alpha d\beta dv' F(\alpha)G(\beta)H(v'), \tag{2.22}$$

where α is the zenith angle, β is the azimuth angle, and v is the ejecta speed. Just to note, at the secondary impact location, the zenith angle will be the same as the ejected zenith angle. However, the azimuth angle (or bearing) will be modified due to travel across the spherical surface, see Section 2.12.

2.7.1 Zenith Distribution Function

For the angular dependent terms $F(\alpha)$ and $G(\beta)$, they technically should depend on speed as well as particle size [e.g., *Rival and Mandeville*, 1999]. For simplicity, we will assume the angular distribution is independent of speed and particle size but will be dependent on impact zenith and azimuth angle with respect to the bearing.

Adopting the zenith and azimuth distributions from *Rival and Mandeville* [1999], we have the following equations: The zenith distribution is given by

$$F(\alpha) = \frac{1}{\sigma\sqrt{2\pi}} \exp\left[-\frac{(\alpha - \alpha_{max})^2}{2\sigma^2}\right], \tag{2.23}$$

where α_{max} is defined as

$$\alpha_{max} = \begin{cases} \frac{\alpha_{max60} - \alpha_{max0}}{\pi/3}\alpha_i + \alpha_{max0} \text{ for } \alpha_i \leqslant \pi/3 = 60^\circ \\ \alpha_{max60} \text{ for } \alpha_i > \pi/3 = 60^\circ \end{cases}, \tag{2.24}$$

for α_i the impact zenith angle, and [see *Miller*, 2017]

$$\alpha_{max0} = \frac{\pi}{6} = 30^\circ, \tag{2.25}$$

$$\alpha_{max60} = \frac{4\pi}{9} = 80^\circ, \tag{2.26}$$

$$\sigma = \frac{\pi}{60} = 3^\circ, \tag{2.27}$$

where the peak ejecta angle is shifted from 30° of zenith for a normal impact to 80° of zenith for oblique impacts ($> 60^\circ$).

Alternative Zenith Distribution: To complete the integral over the zenith distribution, namely

$$\int_{\alpha_0(v)}^{\alpha_1(v)} d\alpha \sin\alpha F(\alpha), \tag{2.28}$$

we need to choose a distribution function for $F(\alpha)$ to allow for analytic solutions. We will therefore look for an alternate distribution from Eq. (2.23), given by the form

$$F(\alpha) = (1-\cos\alpha)^{1/a}\cos^a\alpha, \tag{2.29}$$

where the exponent a can be defined in terms of the peak angle α_{max} as

$$a^2 = \frac{\cos\alpha_{max}}{1-\cos\alpha_{max}} = \frac{\cos\alpha_{max}}{2\sin^2(\alpha_{max}/2)}, \tag{2.30}$$

such that $F'(\alpha_{max}) = 0$ and $F''(\alpha_{max}) < 0$.

In order to compare with experiments for the peak angle α_{max}, we can use Figure 18 of *Gault and Wedekind* [1978] as a proxy to our model of α_{max}, as a function of the azimuth angle. Using a third order polynomial for both fits to the downstream and upstream angles given in Table 2, we arrive at

$$\alpha_{max}(\beta-\beta_i=\pi) = 0.0003\alpha_i^3 - 0.036\alpha_i^2 + 1.5206\alpha_i + 20, \text{ downstream} \tag{2.31}$$

$$\alpha_{max}(\beta-\beta_i=0) = -0.00042\alpha_i^3 + 0.0236\alpha_i^2 + 0.129\alpha_i + 20, \text{ upstream} \tag{2.32}$$

in units of degrees, where β_i is the impact azimuth angle, β is the ejecta azimuth angle, and α_i is the impact zenith angle. For other values of $\beta - \beta_i$, we can write a complete function as

$$\alpha_{max}(\beta) = \alpha_{max}(\beta-\beta_i=\pi)\cdot\sin^2\left(\frac{\beta-\beta_i}{2}\right) + \alpha_{max}(\beta-\beta_i=0)\cdot\cos^2\left(\frac{\beta-\beta_i}{2}\right), \tag{2.33}$$

or rewriting we have

$$\alpha_{max}(\beta) = \frac{\alpha_{max,0}+\alpha_{max,\pi}}{2} - \frac{\alpha_{max,\pi}-\alpha_{max,0}}{2}\cos(\beta-\beta_i), \tag{2.34}$$

and solving for $\beta - \beta_i$, after setting $\alpha_{max}(\beta)$ to zero,

$$\arccos\left(\frac{\alpha_{max,0}+\alpha_{max,\pi}}{\alpha_{max,\pi}-\alpha_{max,0}}\right) = \beta-\beta_i. \tag{2.35}$$

As a simplification, we can approximate the $\cos(\beta-\beta_i)$ term as (note, this is not a Taylor series)

$$\cos(\beta-\beta_i) \sim 1 - \left|\frac{\beta-\beta_i}{\pi/2}\right|, \tag{2.36}$$

for $-\pi \leqslant \beta-\beta_i \leqslant \pi$ such that $\cos\alpha_{max}$ becomes

$$\cos\alpha_{max} \sim \cos\left[\alpha_{max,0} + \frac{\alpha_{max,\pi}-\alpha_{max,0}}{\pi}|\beta-\beta_i|\right] \tag{2.37}$$

Table 2: Cone angles of upstream and downstream of impact derived from Figure 18 of *Gault and Wedekind* [1978].

Impact Zenith Angle	Upstream Zenith Angle	Downstream Zenith Angle
0	20	20
15	24	35
30	35	45
45	28	40
60	13	54
75	-35	66

Using Table 2 as a fit for the peak angle α_{max} is an approximation since the tabular data is only for a specific snapshot of the ejecta at a side view, $90°$ from the impact direction. The zenith distribution should also be a function of the ejecta speed, but we do not make this assumption for the sake of simplicity. According to this model, starting around $60° - 70°$, there is a region of exclusion for a part of the zenith distribution upstream of the impact, see Figure 6.

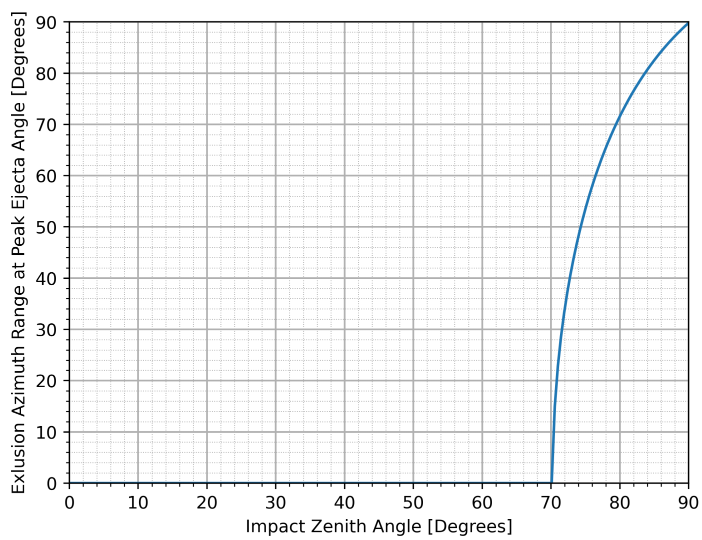

Figure 6: For larger impact angles that are more grazing to the surface, the zenith and azimuth ejecta distributions become asymmetric. Starting at $70°$, the peak ejecta angle α_{max} becomes negative in an exclusion range, as shown in the figure. This means that the $-\alpha_{max} \rightarrow \alpha_{max}$ and $\beta - \beta_i \rightarrow \beta - \beta_i + \pi$. In this model, for impact angles near $90°$, most of the ejecta is concentrated in the downstream direction.

Next, we can do a variable substitution (chosen so the domain of the zenith angle to the new variable goes from $\alpha \in [0, \pi/2]$ to $x \in [0, 1]$)

$$1 - x = \cos\alpha, \tag{2.38}$$

$$dx = \sin\alpha d\alpha, \tag{2.39}$$

so that Eq. (2.28) becomes

$$\int_{x_0(v)}^{x_1(v)} dx x^{1/a} (1-x)^a, \tag{2.40}$$

where the equations $x_0(v)$ and $x_1(v)$ are a linear function of v and an implicit function of the distances D_0 and D_1, respectively. The integral in Eq. (2.40) is the incomplete beta function

$$\int_{x_0(v)}^{x_1(v)} dx x^{1/a} (1-x)^a = \beta(x_1(v); 1/a+1, a+1) - \beta(x_0(v); 1/a+1, a+1). \tag{2.41}$$

Note that the normalization term for $\alpha \in [0, \pi/2]$ is given by

$$\int_0^{\pi/2} d\alpha \sin\alpha F(\alpha) = \beta(1/a+1, a+1) = \frac{\Gamma(1/a+1)\Gamma(a+1)}{\Gamma(a+1/a+2)}, \tag{2.42}$$

which includes ejecta at speeds greater than the escape speed.

For small differences in D_0 and D_1, we can roughly assume small differences[2] in $x_0(v)$ and $x_1(v)$ so that we can write Eq. (2.41) in terms of a derivative, where we evaluate the derivative at the midpoint

$$\begin{aligned}
&\beta(x_1(v); 1/a+1, a+1) - \beta(x_0(v); 1/a+1, a+1) \\
=&\frac{\beta(x_0(v)+\Delta x; 1/a+1, a+1) - \beta(x_0(v); 1/a+1, a+1)}{\Delta x}\Delta x \\
\approx&\Delta x \frac{d}{d(x_0(v))}\beta(x_0(v); 1/a+1, a+1)\Big|_{x_0(v)\to x_0(v)+\Delta x/2} \\
=&\Delta x \left[1 - x_0(v)\right]^a x_0^{1/a}(v)\Big|_{x_0(v)\to x_0(v)+\Delta x/2} \\
=&\Delta x(v)\left[1 - \frac{x_0(v)+x_1(v)}{2}\right]^a \left[\frac{x_0(v)+x_1(v)}{2}\right]^{1/a},
\end{aligned} \tag{2.43}$$

where $\Delta x(v) = x_1(v) - x_0(v)$, and (note, the v's are normalized by v_{esc}, emitted for clarity)

$$x_0(v) = m_0 v + b_0, \tag{2.44}$$

$$x_1(v) = m_1 v + b_1, \tag{2.45}$$

$$\Delta x(v) = (m_1 - m_0)v + b_1 - b_0. \tag{2.46}$$

[2] If Δx is not small, then we can partition the x range into smaller pieces so that Δx is small, which will be the case in almost all circumstances.

The coefficients m_0, m_1 and b_0, b_1 are implicit functions of the distances D_0, D_1. For the $j-$th distance D_j and the $i-$th speed v_i, the m and b coefficients can be written as

$$m^{\pm}_{j,i} = \frac{v_{i+1} - v_i}{x^{\pm}_{j,i+1} - x^{\pm}_{j,i}}, \tag{2.47}$$

$$b^{\pm}_{j,i} = v_i - m^{\pm}_{j,i} \cdot x^{\pm}_{j,i}, \tag{2.48}$$

where

$$x^{\pm}_{j,i} = 1 - \cos\alpha^{\pm}_{j,i}, \tag{2.49}$$

for

$$\cos^2\alpha^{\pm}_{j,i} = \frac{v_i^2 + \tan^2\left(\frac{D_j}{2r_m}\right)(2v_i^2 - 1) \pm \sqrt{v_i^4 + \tan^2\left(\frac{D_j}{2r_m}\right)(2v_i^2 - 1)}}{2v_i^2\left(1 + \tan^2\left(\frac{D_j}{2r_m}\right)\right)}, \tag{2.50}$$

taking the positive root, $\cos\alpha^{\pm}_{j,i} = +\sqrt{\cos^2\alpha^{\pm}_{j,i}}$, since $\alpha \in [0, \pi/2]$. Other useful transformed equations are

$$\tan\left(\frac{D_j}{2r_m}\right) = \frac{2v_i^2(1 - x^{\pm}_{j,i})\sqrt{x^{\pm}_{j,i}(2 - x^{\pm}_{j,i})}}{1 - 2v_i^2 x^{\pm}_{j,i}(2 - x^{\pm}_{j,i})}, \tag{2.51}$$

from Eq. (2.107), and

$$v_i = \frac{1}{\sqrt{2(1 - x^{\pm}_{j,i})\sqrt{x^{\pm}_{j,i}(2 - x^{\pm}_{j,i})}\cot\left(\frac{D_j}{2r_m}\right) + 2x^{\pm}_{j,i}(2 - x^{\pm}_{j,i})}}, \tag{2.52}$$

from Eq. (2.110). Solving for $x^{\pm}_{j,i}$ in either equation, we can now write x explicitly in terms of the distance D and ejecta speed v as

$$x^{\pm}_{j,i} = 1 - \sqrt{\frac{v_i^2 + \tan^2\left(\frac{D_j}{2r_m}\right)(2v_i^2 - 1) \pm \sqrt{v_i^4 + \tan^2\left(\frac{D_j}{2r_m}\right)(2v_i^2 - 1)}}{2v_i^2\left[1 + \tan^2\left(\frac{D_j}{2r_m}\right)\right]}}. \tag{2.53}$$

For a given distance, the domain of x is given by (for v up to 1)

$$x^{\pm}_{j,i} \in \left(1 - \cos\left(\frac{D_j}{4r_m}\right), 1\right), \tag{2.54}$$

and the domain of v is given by

$$v_i \in \begin{cases} \left(\left[1 + \left|\cos\left(\frac{D_j}{2r_m}\right)\right|\cot\left(\frac{D_j}{2r_m}\right) + \sin\left(\frac{D_j}{2r_m}\right)\right]^{-1/2}, 1\right) & \text{for } D_j < \pi r_m \\ \left(\frac{\sqrt{2}}{2}, 1\right) & \text{for } D_j \geqslant \pi r_m \end{cases} \tag{2.55}$$

where the value of $x^{\pm}_{j,i}$ at the minimum of v_i is

$$x^{\pm}_{j,i} = 1 - \sqrt{\frac{1 - \sin\left(\frac{D_j}{2r_m}\right)}{2}} \tag{2.56}$$

The two domains in Eqs. (2.54) and (2.55) define the region of interest, and allow for the integration to begin at the correct outermost boundary lines.

There are three regions of the zenith angle-space, and hence the x-space, where we have:

Region I: For all valid distances D_j and D_{j+1}, use $m^{+}_{j,i}$, $b^{+}_{j,i}$, $m^{+}_{j+1,i}$ and $b^{+}_{j+1,i}$

Region II: For $D_j < \pi r_m$ and all D_{j+1}, use $m^{-}_{j,i}$, $b^{-}_{j,i}$, $m^{+}_{j+1,i}$ and $b^{+}_{j+1,i}$

Region III: For $D_j < \pi r_m$ and $D_{j+1} < \pi r_m$, use $m^{-}_{j,i}$, $b^{-}_{j,i}$, $m^{-}_{j+1,i}$ and $b^{-}_{j+1,i}$

2.7.2 Azimuth Distribution Function

The azimuth distribution shown below is given by [*Rival and Mandeville*, 1999]

$$G(\beta) = \begin{cases} \frac{1}{2\pi}\left[\frac{3\alpha_i}{2\pi - 3\alpha_i}\cos(\beta - \beta_i) + 1\right] & \text{for } \alpha_i \leqslant \pi/3 = 60^\circ \\ \frac{1}{\sigma'\sqrt{2\pi}}\exp\left[-\frac{(\beta-\beta_i)^2}{2\sigma'^2}\right] & \text{for } \alpha_i > \pi/3 = 60^\circ \end{cases}, \tag{2.57}$$

where

$$\sigma' = \frac{\pi}{36} = 5^\circ, \tag{2.58}$$

for β_i the impact azimuth angle + π.

Alternative Azimuth Distribution: The piece-wise function defined in Equation (2.57) for the azimuth distribution is correctly normalized for impact zenith angles $\alpha_i \leqslant 60^\circ$, however for angles greater than 60°, the function is not continuous across the boundary $\beta = 2\pi \to 0$. We would also like a continuous function across the piece-wise boundary as well.

Our proposed azimuth distribution is as follow. We will use the $\alpha_i \leqslant 60^\circ$ functional form in Equation (2.57), but we will have a different large-angle expression. The new azimuth distribution is defined as

$$G(\beta) = \begin{cases} \frac{1}{2\pi}\left[\frac{3\alpha_i}{2\pi - 3\alpha_i}\cos(\beta - \beta_i) + 1\right] & \text{for } \alpha_i \leqslant \pi/3 = 60^\circ \\ \frac{1}{A}\left[\exp\left[-\frac{(\beta-\beta_i-2(\alpha_i-\alpha_{i,0}))}{\pi b}\right] + \exp\left[-\frac{(\beta-\beta_i+2(\alpha_i-\alpha_{i,0}))}{\pi b}\right]\right] & \text{for } \alpha_i > \pi/3 \end{cases}, \tag{2.59}$$

where

$$b = \frac{0.05 - 1}{\pi/2 - \pi/3}(\alpha_i - \alpha_{i,0}) + 1 = \frac{3}{10\pi}(\alpha_i - \alpha_{i,0}) + 1, \tag{2.60}$$

and

$$\alpha_{i,0} = \pi/3. \tag{2.61}$$

For the second case, we empirically include information about the *butterfly pattern* that is seen for highly oblique impact angles [e.g., *Shuvalov*, 2011]. The size of the impactor will affect the spread of the butterfly pattern, but we assume a certain spread profile for all impactor sizes.

The normalization[3] constant for the $\alpha_i > \pi/3$ case is

$$A = \sqrt{b}\pi \left[\text{erf}\left(\frac{\pi + 2(\alpha_i - \alpha_{i,0})}{\sqrt{\pi b}}\right) + \text{erf}\left(\frac{\pi - 2(\alpha_i - \alpha_{i,0})}{\sqrt{\pi b}}\right)\right], \tag{2.62}$$

when integrating $\beta - \beta_i$ from $-\pi$ to π. However, when integrating the outgoing secondary azimuth angle β with respect to the impact azimuth angle β_i when there is an exclusion zone defined by $\pm\Delta\beta_{ez}$, the normalization constant is

$$A = \sqrt{b}\pi \left[\text{erf}\left(\frac{\pi - \Delta\beta_{ez} + 2(\alpha_i - \alpha_{i,0})}{\sqrt{\pi b}}\right) + \text{erf}\left(\frac{\pi - \Delta\beta_{ez} - 2(\alpha_i - \alpha_{i,0})}{\sqrt{\pi b}}\right)\right], \tag{2.63}$$

which is appropriate for any $\alpha_i > \pi/3$ for an exclusion zone $\Delta\beta_{ez}$ given by (using Eq. (2.37) = $\pi/2$)

$$\Delta\beta_{ez} = \begin{cases} \pi\frac{-\alpha_{max,\pi}}{\alpha_{max,0}-\alpha_{max,\pi}}, \text{ for } \alpha_{max,\pi} < 0 \\ 0, \text{ otherwise} \end{cases} \tag{2.64}$$

For $\alpha_i > \pi/3 = 60°$, in order to integrate over a small azimuth range $\beta \in (\beta_0, \beta_1)$

For $\alpha_i \leqslant \pi/3 = 60°$, integrating over a small range $\Delta\beta = \beta_1 - \beta_0$, the integral is given by

$$\begin{aligned} &\frac{1}{2\pi}\int_{\beta_0}^{\beta_1} d\beta \left[\frac{3\alpha_i}{2\pi - 3\alpha_i}\cos(\beta - \beta_i) + 1\right] \\ =&\frac{1}{2\pi}\left[\Delta\beta + \frac{3\alpha_i}{2\pi - 3\alpha_i}\left[\sin(\beta_1 - \beta_i) - \sin(\beta_0 - \beta_i)\right]\right]. \end{aligned} \tag{2.65}$$

Alternative Oblique Impact Azimuth Distribution In favor for a simpler implementation, we can opt for an azimuth distribution given by

$$G(\beta) = \begin{cases} \frac{1}{2\pi}\left[\frac{3\alpha_i}{2\pi - 3\alpha_i}\cos(\beta - \beta_i) + 1\right] \text{ for } \alpha_i \leqslant \pi/3 = 60° \\ \frac{1+\cos(\beta-\beta_i)}{2\pi} \text{ for } \alpha_i > \pi/3 \end{cases}, \tag{2.66}$$

which ignores the *butterfly pattern*, but still includes information about a bias towards the downstream direction of the primary impact.

[3]Please note that this is not the exact normalization. This is assuming that the altitude distribution does not depend on the azimuth, which is not the case. We only include this here to *help* the overall normalization once we calculate it, which will have to be done by a numerical integral.

2.7.3 Speed Distribution Function

The speed distribution $H(v')$ is defined by

$$\int_v^\infty dv' H(v') = v^{-3\mu}, \tag{2.67}$$

which is the speed dependent term of Eq. (2.18). We can then solve the speed distribution explicitly as

$$H(v) = 3\mu v^{-(3\mu+1)}. \tag{2.68}$$

To integrate over the velocity distribution, we must take the results from Section 2.7.1 on the zenith distribution function and combine them with the above integral, giving

$$3\mu \int_{v_0}^{v_1} dv v^{-(3\mu+1)} \Delta x(v) \left[1 - \frac{x_0(v)+x_1(v)}{2}\right]^a \left[\frac{x_0(v)+x_1(v)}{2}\right]^{1/a} \tag{2.69}$$

$$=3\mu \int_{v_0}^{v_1} dv v^{-(3\mu+1)} (\Delta m v + \Delta b)(1 - m_{avg} v - b_{avg})^a (m_{avg} v + b_{avg})^{1/a} \tag{2.70}$$

$$= \int_{v_0}^{v_1} dv H_2(v), \tag{2.71}$$

where

$$\Delta m = m_1 - m_0, \tag{2.72}$$

$$\Delta b = b_1 - b_0, \tag{2.73}$$

$$m_{avg} = \frac{m_0 + m_1}{2}, \tag{2.74}$$

$$b_{avg} = \frac{b_0 + b_1}{2}. \tag{2.75}$$

This integral is related to the Appell F1 multivariate hypergeometric function and cannot be simplified to a finite number of single variable hypergeometric functions for generalized values of the exponent a. At this time, we will defer to integrate this equation numerically, preferably using the Romberg integration method.

Alternatively, we can attempt to generate an approximation similar to what we did in Sections 2.7.1 and 2.7.2. Taking the Taylor expansion of Equation (2.71) about v_{avg} out to the first term, we have (note, the first term drops out of the integral during integration, so the error is of order Δv^3)

$$\int_{v_0}^{v_1} dv H_2(v) \sim \int_{v_0}^{v_1} dv [H_2(v_{avg}) + H_2'(v_{avg})(v - v_{avg}) + \ldots], \tag{2.76}$$

$$= \Delta v H_2(v_{avg}),$$

$$= 3\mu \Delta v v_{avg}^{-(3\mu+1)} (\Delta m v_{avg} + \Delta b)(1 - m_{avg} v_{avg} - b_{avg})^a (m_{avg} v_{avg} + b_{avg})^{1/a}, \tag{2.77}$$

where

$$\Delta v = v_1 - v_0, \tag{2.78}$$

$$v_{avg} = \frac{v_0 + v_1}{2}. \tag{2.79}$$

2.7.4 Speed Bin Centers

The speed bin centers of a bin defined by a minimum and maximum speed, v_{min} and v_{max}, are not simply the average of the bin edges. The correct center is weighted by the speed distribution, which in this case is a power-law, see Equation (2.68). An additional weighting can be included, either by the momentum $\sim v$ or the energy $\sim v^2$, so that the bin centers are given by

$$v_M = \frac{\int_{v_{min}}^{v_{max}} dv \cdot v f(v)}{\int_{v_{min}}^{v_{max}} dv \cdot f(v)}, \tag{2.80}$$

weighted by the momentum, and

$$v_E = \sqrt{\frac{\int_{v_{min}}^{v_{max}} dv \cdot v^2 f(v)}{\int_{v_{min}}^{v_{max}} dv \cdot f(v)}}, \tag{2.81}$$

weighted by the energy. Taking $f(v) = 3\mu v^{-(3\mu+1)}$, we have

$$v_M = \frac{3\mu}{3\mu - 1} \frac{v_{min}^{-3\mu+1} - v_{max}^{-3\mu+1}}{v_{min}^{-3\mu} - v_{max}^{-3\mu}}, \tag{2.82}$$

and

$$v_E = \sqrt{\frac{3\mu}{2 - 3\mu} \frac{v_{max}^{-3\mu+2} - v_{min}^{-3\mu+2}}{v_{min}^{-3\mu} - v_{max}^{-3\mu}}}. \tag{2.83}$$

2.7.5 Normalization Term

In order to relate to the secondary mass ejected faster than v, we need the normalization term $\mathcal{M}$ such that

$$M(> v) = \mathcal{M}(\alpha_i, U_i) \int_v^\infty \int_0^{2\pi} \int_0^{\pi/2} \sin\alpha d\alpha d\beta dv' F(\alpha) G(\beta) H(v'). \tag{2.84}$$

Solving for $\mathcal{M}$ and performing the integral over speed v', we have

$$\mathcal{M}(\alpha_i, U_i) = \frac{C_4 m [U_i \Theta(\alpha_i)]^{3\mu} \left(\frac{\delta}{\rho}\right)^{3\nu - 1}}{\mathcal{G}(\alpha_i)}, \tag{2.85}$$

where $\mathcal{G}$ is given by ($x = \beta - \beta_i$)

$$\mathcal{G}(\alpha_i) = \int_{-(\pi-\Delta\beta_{ez})}^{\pi-\Delta\beta_{ez}} dx G(x+\beta_i) \frac{\Gamma(1/a+1)\Gamma(a+1)}{\Gamma(a+1/a+2)}, \tag{2.86}$$

$$= 2\int_{0}^{\pi-\Delta\beta_{ez}} dx G(x+\beta_i) \frac{\Gamma(1/a+1)\Gamma(a+1)}{\Gamma(a+1/a+2)}, \tag{2.87}$$

where $\Delta\beta_{ez}$ and a are given in Eq. (2.64) and Eq. (2.30), respectively. Recall, that a is given by

$$a^2 = \frac{\cos\alpha_{max}}{1-\cos\alpha_{max}} = \frac{\cos\alpha_{max}}{2\sin^2(\alpha_{max}/2)}, \tag{2.88}$$

and where α_{max} is given by

$$\alpha_{max} = \alpha_{max,0} + \frac{\alpha_{max,\pi} - \alpha_{max,0}}{\pi}|x|. \tag{2.89}$$

The $\mathcal{G}$ pre-normalization term can be computed using your favorite numerical integration method, such as Romberg integration.

2.8 Meteoroid Projectile Mass Distribution

From the MEM3 User Guide , we get the $g(m)$ flux of meteoroids larger than a limiting mass m, originally from *Grün et al.* [1985]. The Grün interplanetary flux equation is given by

$$g(m) = (c_4 m^{\gamma_4} + c_5)^{\gamma_5} + c_6(m + c_7 m^{\gamma_6} + c_8 m^{\gamma_7})^{\gamma_8} + c_9(m + c_{10} m^{\gamma_9})^{\gamma_{10}}, \tag{2.90}$$

where the constants are $c_4 = 2.2\times10^3$, $c_5 = 15$, $c_6 = 1.3\times10^{-9}$, $c_7 = 10^{11}$, $c_8 = 10^{27}$, $c_9 = 1.3\times10^{-16}$, $c_{10} = 10^6$; and the exponents are $\gamma_4 = 0.306$, $\gamma_5 = -4.38$, $\gamma_6 = 2$, $\gamma_7 = 4$, $\gamma_8 = -0.36$, $\gamma_9 = 2$, and $\gamma_{10} = -0.85$. Eq. 2.90 is applied to MEM's mass range and is shown in Figure 7.

The mass flux $dg(m)/dm$ and Eq. 2.18 should be integrated over the mass range $m_{min} = 10^{-6}$ g to $m_{max} = 10^1$ g in order to account for all impactor mass sizes, which we call G_m given as

$$G_m = \int_{m_{min}}^{m_{max}} dm \frac{dg(m)}{dm} m. \tag{2.91}$$

The mass flux $dg(m)/dm$ can be fit to a double power law

$$\frac{dg(x)}{dx} = \frac{1}{ax^b + cx^d}, \tag{2.92}$$

where the fit parameters are shown in Figure 8, using a log-log scale to capture the small and large masses correctly.

To integrate Eq. (2.91), we use the following solutions

$$\int dx \frac{x}{ax^b + cx^d} = -\frac{1}{a(b-2)x^{b-2}}\,{}_2F_1\left[1, \frac{b-2}{b-d}; \frac{b-2}{b-d}+1; -\frac{c}{a}x^{d-b}\right], \tag{2.93}$$

$$= -\frac{1}{c(d-2)x^{d-2}}\,{}_2F_1\left[1, \frac{d-2}{d-b}; \frac{d-2}{d-b}+1; -\frac{a}{c}x^{b-d}\right], \tag{2.94}$$

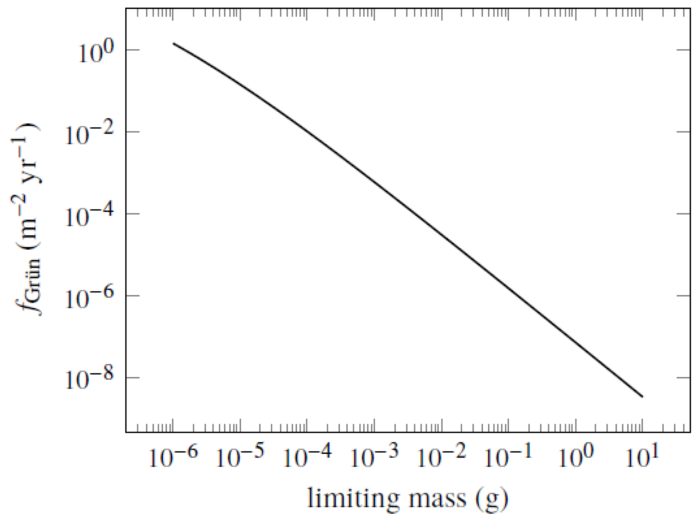

Figure 7: The Grün interplanetary meteoroid flux as a function of limiting particle mass [*Moorhead et al.*, 2019, Figure 1].

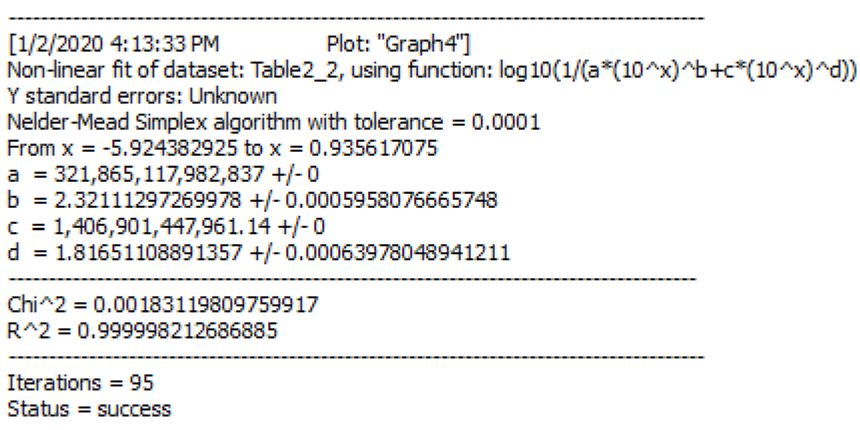

```
[1/2/2020 4:13:33 PM          Plot: "Graph4"]
Non-linear fit of dataset: Table2_2, using function: log10(1/(a*(10^x)^b+c*(10^x)^d))
Y standard errors: Unknown
Nelder-Mead Simplex algorithm with tolerance = 0.0001
From x = -5.924382925 to x = 0.935617075
a  = 321,865,117,982,837 +/- 0
b  = 2.32111297269978 +/- 0.0005958076665748
c  = 1,406,901,447,961.14 +/- 0
d  = 1.81651108891357 +/- 0.00063978048941211
--------------------------------------------------------------------------
Chi^2 = 0.00183119809759917
R^2 = 0.999998212686885
--------------------------------------------------------------------------
Iterations = 95
Status = success
```

Figure 8: Non-linear fit of Figure 7 with Eq. 2.92 in SciDAVis, giving the constants for a, b, c, and d.

where Eq. 2.93 is more appropriate for small x if $d - b > 0$ and Eq. 2.94 is more appropriate for large x if $d - b > 0$. If the sign of $d - b$ is flipped, then the small and large scale equations are swapped.

2.9 Meteoroid Projectile Density Distribution

The meteoroid density has two components, a low and a high density contribution, as shown in Figure 9. To take into account this particular distribution in computing the particle flux mass spectrum, we should integrate Figure 9 against Eq. 2.18. Since the meteoroid density components can be written in terms of log-normal distributions

$$F_\delta(x) = \frac{A}{\sigma\sqrt{2\pi}x}\exp\left[-\frac{(\ln x-\mu_\delta)^2}{2\sigma^2}\right], \tag{2.95}$$

the integration entails computing the moments of a log-normal distribution. The α-moment is given by

$$F_\delta^\alpha(A,\mu_\delta,\sigma) = A\exp\left(\alpha\mu_\delta+\frac{1}{2}\alpha^2\sigma^2\right). \tag{2.96}$$

Inserting these results into Eq. 2.18, the functional form of the projectile density contribution can be written as

$$F_\delta = F_\delta^{3\nu-1}(A_{low},\mu_{low},\sigma_{low}) + F_\delta^{3\nu-1}(A_{high},\mu_{high},\sigma_{high}), \tag{2.97}$$

where the fit parameters for the low and high density components are shown in Figures 10 and 11. Since the meteoroid density is given in units of *fraction per 50 kg m*$^{-3}$, we need to divide the A constants by 50 in order to give correct units.

2.10 Meteoroid Projectile Speed and Angle Distribution

MEM3 gives the incoming meteoroid flux (in units of # per km^2 per year) in terms of the speed U and both azimuth θ and altitude ϕ angles for a location on the Moon. At the moment, since we are assuming azimuthally symmetric ejecta, we will sum over all θ azimuthal angles to simplify our calculation. In the future, we plan to incorporate azimuthal dependence for oblique impacts by including the azimuthal dependence of the ejecta blanket. The ϕ angle in MEM3 corresponds to our α angle, which is the impact angle with respect to the horizon. There are 36 ϕ bins[4] and 40 speed bins, after integrating over the 72 θ bins for each ϕ bin.

2.11 Secondary Ejecta Distance, Speed, & Angle

We would like to relate the distance from the meteorite impact to the secondary ejecta impact site by the secondary ejecta speed v and angle γ from zenith. If we assume the Moon is a perfect sphere with no atmosphere, we can calculate this distance by following the elliptical path the ejecta makes. The semi-major axis and eccentricity of the elliptical orbit are given by[5]

$$\frac{a}{r_m} = \frac{1}{2\left(1-\frac{v^2}{v_{esc}^2}\right)}, \tag{2.98}$$

[4] Half of the ϕ bins will always be zero, since they are below the horizon, so they can be ignored.
[5] See Eqs. 4.30 and 4.32 from http://www.braeunig.us/space/orbmech.htm.

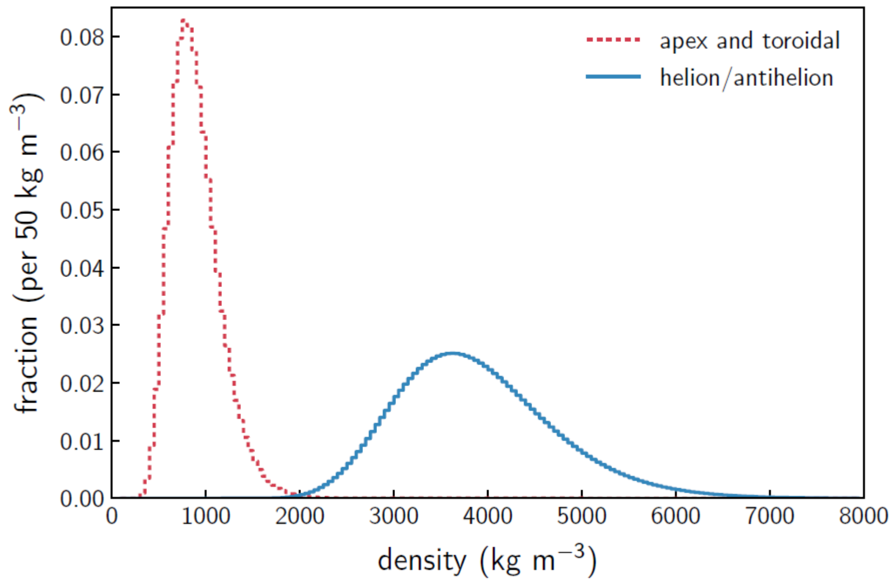

Figure 9: Meteoroid density distribution according to the MEM3 User Guide. The apex and toroidal meteoroid sources constitute the low-density population, while the helion/antihelion source constitutes the high-density population. Each set of densities follows a log-normal distribution [c.f. Figure 11, *Moorhead et al.*, 2019].

```
--------------------------------------------------------------------------------
[1/2/2020 5:16:00 PM            Plot: "Graph5"]
Non-linear fit of dataset: Table3_2, using function: log10(a/((10^x)*s*2.506628275)*exp(-(x*ln(10)-m)^2/(2*s^2)))
Y standard errors: Unknown
Scaled Levenberg-Marquardt algorithm with tolerance = 0.0001
From x = 2.097 to x = 3.902
a  = 53.839135327051 +/- 0.82189223780795
s  = 0.294917539134767 +/- 0.000210957288819632
m  = 6.7346464600191 +/- 0.00131007263737737
--------------------------------------------------------------------------------
Chi^2 = 0.305039664208057
R^2 = 0.999894109124399
--------------------------------------------------------------------------------
Iterations = 0
Status = success
--------------------------------------------------------------------------------
```

Figure 10: Non-linear fit of the low density profile in Figure 9 with Eq. 2.95 in SciDAVis, giving the constants for $a \to A$, $s \to \sigma$, and $m \to \mu_\delta$.

where $r_m = 1737.1$ km is the radius of the Moon and $v_{esc} = 2.38$ km/s is the Moon's escape velocity, and

$$e = \sqrt{\left(\frac{2v^2}{v_{esc}^2} - 1\right)^2 \sin^2\gamma + \cos^2\gamma}, \tag{2.99}$$

```
--------------------------------------------------------------------------------
[1/2/2020 5:19:18 PM            Plot: "Graph6"]
Non-linear fit of dataset: Table4_2, using function: log10(a/((10^x)*s*2.506628275)*exp(-(x*ln(10)-m)^2/(2*s^2)))
Y standard errors: Unknown
Scaled Levenberg-Marquardt algorithm with tolerance = 0.0001
From x = 2.096910013 to x = 3.901730692
a  = 39.742506482046 +/- 1.58430260083343
s  = 0.221066131940955 +/- 0.00039359322394943
m  = 8.26026111215463 +/- 0.00352064330966803
--------------------------------------------------------------------------------
Chi^2 = 5.98458401110512
R^2 = 0.999293469696896
--------------------------------------------------------------------------------
Iterations = 0
Status = iteration is not making progress towards solution
--------------------------------------------------------------------------------
```

Figure 11: Non-linear fit of the high density profile in Figure 9 with Eq. 2.95 in SciDAVis, giving the constants for $a \to A$, $s \to \sigma$, and $m \to \mu_\delta$.

where we employed the fact that the gravity of the Moon is $g = GM/r_m^2$ and the escape velocity is related by $v_{esc} = \sqrt{2gr_m}$. The third equation we need gives the location in the elliptical orbit by the angle β from the perilune, the semi-major axis a, and the eccentricity e by

$$r = \frac{a(1-e^2)}{1+e\cos\beta}. \tag{2.100}$$

Solving for $\cos\beta$ in Eq. 2.100, we have

$$\cos\beta = \frac{1}{e}\left(\frac{a(1-e^2)}{r} - 1\right). \tag{2.101}$$

In addition, we also need the equation for $\sin\beta$, which is given by (using a right triangle)

$$\sin\beta = \frac{1}{e}\sqrt{e^2 - \left[\frac{a(1-e^2)}{r} - 1\right]^2}, \tag{2.102}$$

so that $\tan\beta$ is

$$\tan\beta = \frac{\sqrt{e^2 - \left[\frac{a(1-e^2)}{r} - 1\right]^2}}{\frac{a(1-e^2)}{r} - 1}. \tag{2.103}$$

We found that the distance the secondary ejecta travels is given by the arc length of Moon the orbit travels greater than the radius of the Moon:

$$D = 2(\pi - \beta)r_m, \tag{2.104}$$

or solving for the angle β,

$$\beta = \pi - \frac{D}{2r_m}. \tag{2.105}$$

Using Eqs. 2.98 and 2.99, we can write

$$\frac{a}{r_m}(1-e^2) = 2\frac{v^2}{v_{esc}^2}\sin^2\gamma, \tag{2.106}$$

so Eq. 2.103 becomes [c.f., Eq. (1) of *Vickery*, 1986]

$$\tan\left(\frac{D}{2r_m}\right) = \frac{2\frac{v^2}{v_{esc}^2}\sin\gamma\cos\gamma}{1-2\frac{v^2}{v_{esc}^2}\sin^2\gamma} = \frac{\frac{v^2}{v_{esc}^2}\sin(2\gamma)}{\frac{v^2}{v_{esc}^2}[\cos(2\gamma)-1]+1} = \frac{2\frac{v^2}{v_{esc}^2}\tan\gamma}{1+(1-2\frac{v^2}{v_{esc}^2})\tan^2\gamma}. \tag{2.107}$$

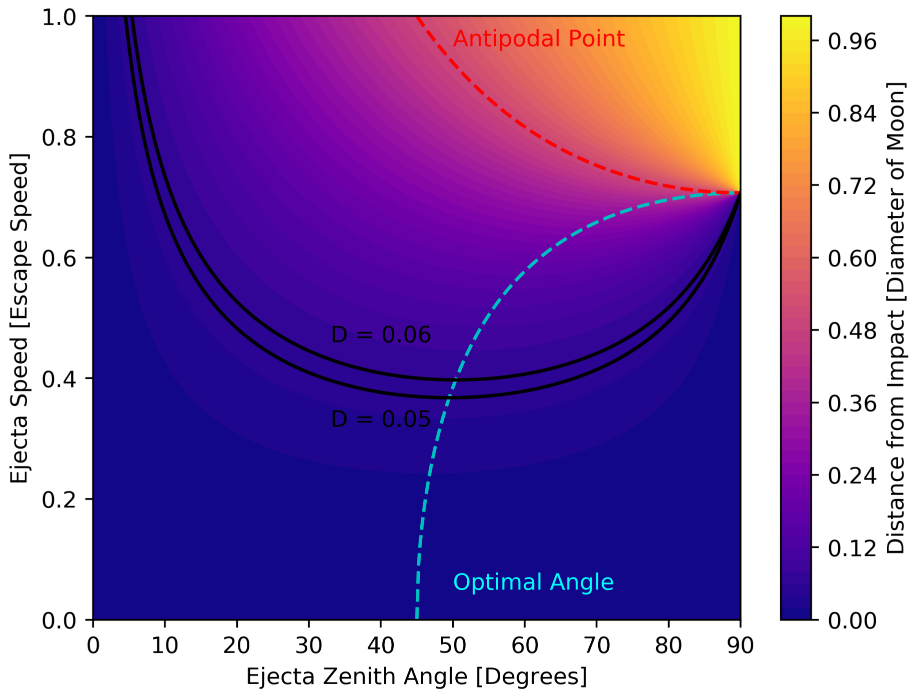

Figure 12: The color gradient shows the distance a projectile goes with a given ejected speed and zenith angle. The cyan dashed line gives the optimal angle for a given speed to reach the furthest distance, i.e., Eq. (2.114). The red dashed line shows for which pairs of speeds and zenith angles are required to hit the antipodal point. As an example, all ejecta with speed and angle pairs between the two black curves will reach a location between 0.05 and 0.06 lunar circumference units away, using Eq. (2.110).

For $D \ll 2r_m$, the optimum angle that gives the smallest velocity needed is $45°$. In other words, for a given velocity, the greatest distance is found by taking $\gamma = 45°$. However, if the distance D is roughly the same order as the diameter of the Moon $2r_m$, $(D > 0.01 \times 2r_m)$, then the optimal angle from zenith is greater than $45°$, i.e. a shallower angle to the horizon. This is because at large velocities, the curvature of the Moon comes into play. For larger velocities, there are also angles γ that cannot reach a distance D. Allowable angles (in radians) that can travel a distance D are defined by

$$\gamma > \frac{D}{4r_m}. \tag{2.108}$$

In other words, the maximum distance the ejecta can reach for a given angle is

$$D = 4\gamma r_m. \tag{2.109}$$

For example, from this equation we can conclude that for $\gamma < 45°$, the ejecta will not reach the antipodal point, see Figure 12.

Solving for v we have

$$\frac{v}{v_{esc}} = \frac{+1}{\sqrt{\sin(2\gamma)\left(\cot\left(\frac{D}{2r_m}\right) + \tan\gamma\right)}} = \frac{+1}{\sqrt{1 + \sin(2\gamma)\cot\left(\frac{D}{2r_m}\right) - \cos(2\gamma)}}. \tag{2.110}$$

We can also solve for the zenith angle γ, given by

$$\cot\gamma = x^2\cot\left(\frac{D}{2r_m}\right) \pm \sqrt{x^4\cot^2\left(\frac{D}{2r_m}\right) + (2x^2 - 1)}, \tag{2.111}$$

where $x = v/v_{esc}$. Solving for the discriminant, the minimum x can be for a given distance D is

$$x_{min}^2 = \tan^2\left(\frac{D}{2r_m}\right)\left[\csc\left(\frac{D}{2r_m}\right) - 1\right], \tag{2.112}$$

$$= \frac{\tan\left(\frac{D}{2r_m}\right)}{\tan\left(\frac{\pi}{4} - \frac{D}{4r_m}\right)}. \tag{2.113}$$

Plugging into Equation 2.111, the optimal angle from zenith is given by

$$\cot\gamma_{opt} = \sec\left(\frac{D}{2r_m}\right) - \tan\left(\frac{D}{2r_m}\right), \tag{2.114}$$

$$= \tan\left(\frac{\pi}{4} - \frac{D}{4r_m}\right).$$

Solving for γ_{opt} we have

$$\gamma_{opt} = \frac{\pi + D/r_m}{4}, \tag{2.115}$$

which is valid for $D \leqslant r_m$. For larger distances, the optimal zenith angle is $\pi/2$. In terms of x, we have

$$\cos(2\gamma_{opt}) = \frac{x^2}{x^2 - 1}. \tag{2.116}$$

Once $D > \pi r_m$, the optimal angle is $\gamma = 90°$, i.e., parallel to the horizon. For small distances $D \ll 2r_m$, the optimal angle is $\gamma = 45°$, as mentioned above.

The distance traveled for the optimal angle as a function of speed is

$$\frac{D}{2r_m} = \arcsin\left(\frac{x^2}{1 - x^2}\right). \tag{2.117}$$

2.11.1 Coriolis Force

The Coriolis force on secondary ejecta may also affect the ground path. To estimate the strength of the Coriolis force, the greatest speed due to the rotation of the Moon is at the equator, given by

$$v_c = \frac{2\pi r_m}{T} = \frac{2\pi * 1737.1 \text{ km}}{27.322 \text{ days}} = 4.62 \text{ m/s}. \tag{2.118}$$

Therefore, we can ignore the Coriolis force if the ejecta speed v is greater than roughly $\sim 10 - 15 \times v_c$, or about 46 m/s to 70 m/s. This translates into ejecta distances less than 3 km, which at those small distances the Coriolis force should not cause an effect anyways. So in general, we conclude that we can ignore the Coriolis force all together.

To quantify this conclusion, let us compute the Rossby number

$$R_o = \frac{v}{fL}. \tag{2.119}$$

If we assume an ejecta angle of $45°$, then plotting D as a function of v in Eq. 2.107 shows that $D \to L \sim v^2$. Taking our example above for $v = 70$ m/s, $L = 3$ km, and $f = 2T$ to solve for A, we find that the Rossby number for secondary ejecta on the Moon is

$$R_o = \frac{A}{fv}, \tag{2.120}$$

where $A = 1.63$ m/s^{2,6}, $f = 5.328 \times 10^{-6}$ rad/s, and v is in units of m/s. In order to have $R_o \sim 1$ (small R_o means the Coriolis forces cannot be ignored), we would need $v > 306$ km/s, which far exceeds the escape speed. The smallest R_o can ever be is $R_o \sim 128$ when taking $v \to v_{esc}$. Therefore, we feel confident in our omission of the Coriolis force.

2.12 Distance and Bearing

Given two latitude-longitude points on a sphere, (ϕ_1, θ_1) and (ϕ_2, θ_2), we can compute the distance and bearing following Chris Veness's webpage[7].

The distance D is given by the equation

$$\tan\left(\frac{D}{2r_m}\right) = \sqrt{\frac{a}{1-a}}, \tag{2.121}$$

where a is given by

$$a = \sin^2(\Delta\phi/2) + \cos\phi_1 \cos\phi_2 \sin^2(\Delta\lambda/2), \tag{2.122}$$

for $\Delta\phi = \phi_2 - \phi 1$ and $\Delta\lambda = \lambda_2 - \lambda_1$. Solving for the distance and simplifying, we have

$$D = 2r_m \arcsin(\sqrt{a}), \tag{2.123}$$

[6] Curiously, this is basically the acceleration due to gravity on the Moon.
[7] https://www.movable-type.co.uk/scripts/latlong.html

or

$$D = 2r_m \arccos(\sqrt{1-a}). \tag{2.124}$$

Other useful expressions involving trigonometric functions of D/r_m are

$$\sin(D/r_m) = 2\sqrt{a(1-a)}, \tag{2.125}$$
$$\cos(D/r_m) = 1 - 2a, \tag{2.126}$$
$$\tan(D/r_m) = \frac{2\sqrt{a(1-a)}}{1-2a}. \tag{2.127}$$

Eq. (2.121) is the shortest distance between two coordinate points. For the long-distance, use

$$\tan\left(\pi - \frac{D}{2r_m}\right) = -\tan\left(\frac{D}{2r_m}\right) = \sqrt{\frac{a}{1-a}}. \tag{2.128}$$

The initial bearing θ (from due East) is given by the following equation (assuming the short-distance):

$$\tan\theta_{i(1,2)} = \frac{\sin\Delta\lambda\cos\phi_2}{\cos\phi_1\sin\phi_2 - \sin\phi_1\cos\phi_2\cos\Delta\lambda}. \tag{2.129}$$

To find the final bearing (assuming the short-distance), swap $\phi_1 \longleftrightarrow \phi_2$ and $\lambda_1 \longleftrightarrow \lambda_2$ and reverse the angle such that

$$\theta_{f(1,2)} = (\theta_{i(2,1)} + \pi) \mod 2\pi. \tag{2.130}$$

In order to compute the initial and final bearing for the long-distance trajectory, add π and then mod by 2π to Eqs. (2.129) and (2.130). In other words, swap initial and final bearings $\theta_{i(1,2)} \longleftrightarrow \theta_{f(1,2)}$.

We can also get the final latitude and longitude if we are given the distance D and bearing θ from the starting location. The latitude and longitude are given by

$$\phi_2 = \arcsin\left[\sin\phi_1\cos(D/r_m) + \cos\phi_1\sin(D/r_m)\cos\theta\right], \tag{2.131}$$
$$\lambda_2 = \lambda_1 + \arctan\left[\frac{\sin\theta\sin(D/r_m)\cos\phi_1}{\cos(D/r_m) - \sin\phi_1\sin\phi_2}\right]. \tag{2.132}$$

3 NASA SP-8013 Meteoroid Environment Model - 1969

The NASA SP-8013 Meteoroid Environment Model [*Cour-Palais*, 1969], is a document published in 1969 that describes the meteoroid and lunar ejecta environment of cometary origin with masses between 10^{-12} g and 1 g. The flux-mass models and the associated density and velocity characteristics are for engineering applications in the design of space vehicles for near-Earth orbit, cis-lunar, lunar orbit, and lunar surface missions.

Our aim is to provide an updated specification to NASA SP-8013 for the lunar impact ejecta environment. Until the update is finished, DSNE points to Figure 10

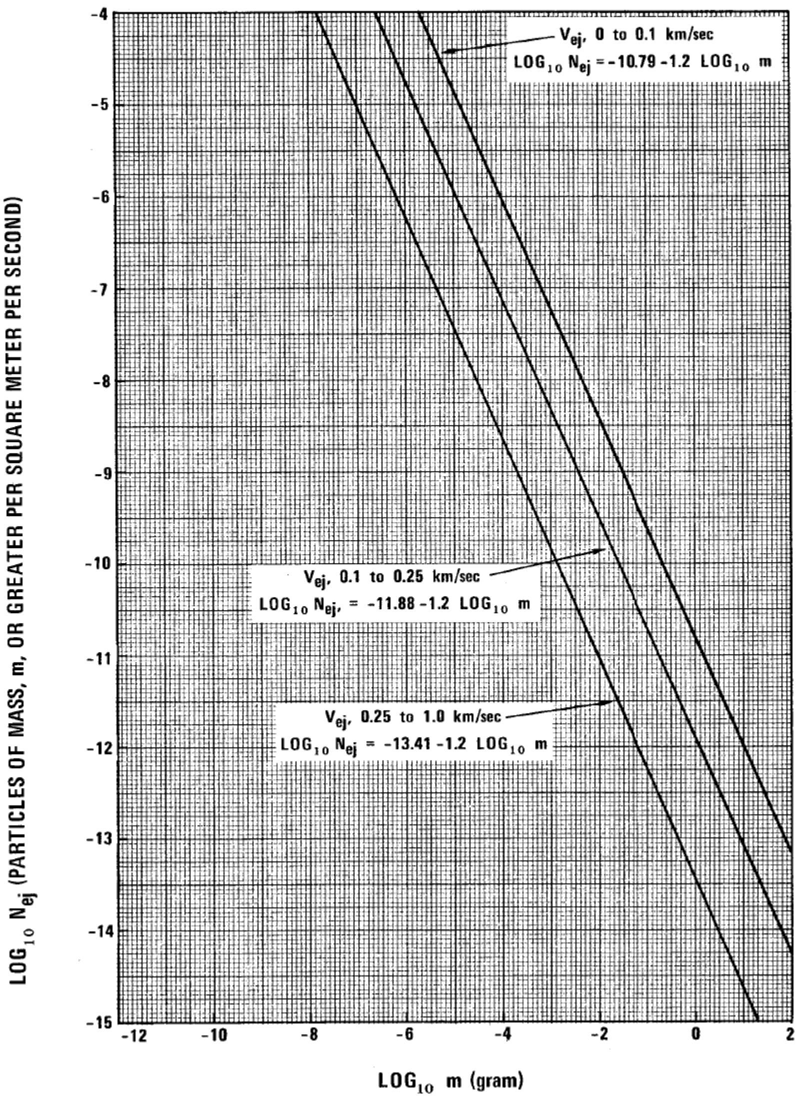

Figure 13: Average cumularive lunar ejecta flux-mass distribution for each of three ejecta velocity intervals [*Cour-Palais*, 1969].

(shown here in Figure 13) of *Cour-Palais* [1969] for lunar ejecta. The results that follow from Sections **??** and 2 will be verified against NASA SP-8013. We already anticipate that our new environments will be more benign (e.g., [*Bjorkman and Christiansen*, 2019, pointing out that 50 J is the critial energy]), however to what degree from our analysis is yet to be determined. We also plan to provide output in terms of penetrating flux as a function of critical kinetic energy, as comparison to Figure 5 of *Bjorkman and*

Christiansen [2019], to aid in risk assessment of lunar impact ejecta.

Our ultimate goal in providing an updated environment definition is to have an output in the same format as MEM 3's igloo files (see Section 3.4.4 of *Moorhead et al.* [2019]). This will allow for current analysis tools already familiar with MEM 3 to ingest our new environments without modification to those tools.

3.1 Comparison of Scaling Laws of New and Old Ejecta Models

In this section we dive into the comparison between the scaling laws assumed in the secondary ejecta environment of the Housen & Holsapple 2011 model and the NASA SP-8013 model, i.e., *Zook* [1967]. Previously in Section 4.1, the scaling law equation from *Housen and Holsapple* [2011] has the following relation:

$$\bar{m}_{\mathsf{HH11}}(>v) \sim \left(\frac{U}{v}\right)^{3\mu}, \tag{3.1}$$

where $\bar{m}_{\mathsf{HH11}}(>v)$ is the secondary ejecta greater than the ejecta speed v, and U is the impactor speed. We are ignoring any density dependence of the target or impactor. The μ index depends on the target properties (such as strength/porosity).

On the other hand, from *Zook* [1967] we have (which is based on laboratory data of impacts in solid basalt):

$$\bar{m}_{\mathsf{Z67}}(>v) \sim U^{-2\beta\gamma}\left[G(v)\right]^{1-\frac{3}{\alpha}(1+\gamma)}, \tag{3.2}$$

where γ is the power-law index of the cumulative flux-mass relation of the primaries, α depends on the target properties, and the function $G(v)$ [from Figure 10 of *Gault et al.*, 1963] relates the dependence of ejecta mass and ejecta speed (which is assumed to be a single-valued function, such that an inverse can be defined).

According to *Zook* [1967], the value of α ranges between 0.3 and 0.7 where a more general restriction is $\alpha < 1$ from *Gault et al.* [1963]. In addition, $\beta \leqslant 1$ [*Gault et al.*, 1963] for basalt targets and might even be $\beta < 0.88$ by empirical scaling laws in alluvium. The value for the primary flux-mass index γ depends on analysis of the comets and asteroids, typically measured at/from Earth. *Zook* [1967] showed that γ depends on the primary mass m (in grams) such that

$$\begin{aligned} \gamma &= -0.3,\ 10^{-14} \leqslant m < 10^{-8} \\ \gamma &= -1.0,\ 10^{-8} \leqslant m < 10^{-2.15} \\ \gamma &= -1.34,\ 10^{-2.15} \leqslant m < \infty, \end{aligned} \tag{3.3}$$

whereas in our new ejecta model, we employ *Grün et al.* [1985]. Fitting a single power-law to the Grün interplanetary fluxes gives (in the range $10^{-6} < m < 10^{1}$)

$$\gamma \approx -1.25, \tag{3.4}$$

which seems to agree with the index range from *Zook* [1967].

In theory, in order for the secondary fluxes to be finite, we require the primary flux index γ to be $\gamma < -1$, otherwise we need a finite upper limit to the size of the primaries. Interestingly, if $\gamma = -1$, then the secondary fluxes suggested by Zook in Equation (3.2) stop being dependent on the target material.

There is a third ejecta model that can be found in the literature that is based on fitting laboratory data and producing scaling laws given by *Koschny and Grün* [2001]. Without going into too much detail, the scaling law equation can be summarized as

$$\bar{m}_{\mathsf{KG01}}(>v) \sim m^{b-1}\frac{U^{2b}}{v^{\gamma_1}}, \tag{3.5}$$

where both b and γ_1 depend on target properties. For basalt targets, $b = 1.02$ [*Moore et al.*, 1963]. For regolith-type targets $\gamma_1 = 1.2$ and for solid- (basalt) type target $\gamma_1 = 2$ [*Krivov et al.*, 2003].

4 Analytic Study of Secondary Lunar Ejecta

In this section, we dive into a *back-of-the-envelope* approach to understanding the secondary ejecta on the Moon. We begin by first defining the expected total mass of ejecta that is produced by an impact (or class of impacts) in Section 4.1, first discussed in Section 2.6. We then count secondary ejecta produced over the entire surface of the Moon that reaches our particular region of interest, discussed in Section 4.2.

The purpose of doing an analytic study of the secondary lunar ejecta is to compare with our computer simulations and to see mathematically what drives the secondary ejecta environment.

4.1 Total Ejected Mass

From *Housen and Holsapple* [2011], we can compute the mass ejected faster than v in terms of impactor properties, given by (copying Equation (2.18) here for convenience))

$$M(v;\rho;m,\delta,U,\alpha) = M(>v) = C_4 m\left[\frac{v}{U\Theta(\alpha)}\left(\frac{\rho}{\delta}\right)^{\frac{3\nu-1}{3\mu}}\right]^{-3\mu}, \tag{4.1}$$

where

- v: secondary ejecta speed,
- ρ: target density,
- m: projectile mass,
- δ: projectile density,
- U: projectile speed,
- α: projectile impact angle (from horizon),

and

$$C_4 = \frac{3k}{4\pi} C_1^{3\mu}, \tag{4.2}$$

where the constants k, C_1, ν, and μ depend on the specific material properties, see Table 3 of *Housen and Holsapple* [2011]. We will assume that $\Theta(\alpha) = 1$ for now (i.e., all impacts are normal to the surface), but will reintroduce this dependence later.

Given that we have a mass distribution and density distribution of primary impactors that are independent of the impact speed and other parameters, we can integrate these out. The mass term is given by (from Equation (2.91))

$$G_m = \int_{m_{min}}^{m_{max}} dm \frac{dg(m)}{dm} m. \tag{4.3}$$

where $\frac{dg(m)}{dm}$ is the derivative of the Grün interplanetary flux in Equation (2.90).

Assuming that the density distribution is log-normal, the density term is given by (from Equation (2.96))

$$F_\delta^\alpha(A, \mu_\delta, \sigma) = A \exp\left(\alpha\mu_\delta + \frac{1}{2}\alpha^2\sigma^2\right). \tag{4.4}$$

We then multiply Equation (4.1) by the primary meteor flux f_p (in number per area per time) so that we have

$$M_p(> v) = \frac{C_4 G_m F_\delta^{3\nu-1}}{\rho^{3\nu-1}} f_p \left(\frac{U}{v}\right)^{3\mu}, \tag{4.5}$$

where we will use $\nu = 0.4$ and $\mu = 0.4$ for the lunar regolith. The units of $M_p(> v)$ is now mass per impact area per time.

4.2 Estimated Secondary Ejecta at a ROI with Normally Impacting Primaries

In order to integrate over the entire Moon, we imagine the region-of-interest (ROI) to be centered on the z-axis of a spherical coordinate system[8] with the radius of the Moon r_m. Therefore, this distance from the center of the ROI is defined as $D = \theta r_m$, where θ is the angle from the z-axis. The azimuthal angle is given by ϕ, defined to rotate in the right-handed sense from the x-axis.

The differential surface area is then given by

$$dA = r_m^2 \sin\theta d\theta d\phi = r_m \sin(D/r_m) dD d\phi. \tag{4.6}$$

When integrating over the distance, we will put a placeholder function D_{min} and D_{max} which can be constant in the ROI distance D or the secondary ejecta speed v and depend on the other.

We can back out the secondary ejecta speed distribution $H(v)$ in Equation (4.5) by employing the definition given in Equation (2.68)

[8] When we have to worry about latitudinal effects, we will need to adjust this definition.

$$H(v) = 3\mu v^{-(3\mu+1)}, \tag{4.7}$$

such that

$$\int_v^\infty dv' H(v') = v^{-3\mu}. \tag{4.8}$$

The corresponding speeds[9] that reach a particular ROI of radius r_{ROI} (or diameter ΔD) at a distance D can be computed by

$$\mathcal{V}(D) = \int_{v(D_0)}^{v(D_1)} dv' H(v'), \tag{4.9}$$

$$= v(D_0 = D - r_{ROI})^{-3\mu} - v(D_1 = D + r_{ROI})^{-3\mu}. \tag{4.10}$$

In the limit as $\Delta D \to 0$, or $\Delta D / r_m \ll 1$, we can approximate $\mathcal{V}$ as

$$\mathcal{V}(D) = -\Delta D f_v'(D) + \mathcal{O}(\Delta D^3), \tag{4.11}$$

with an error[10] proportional to $\Delta D^3 f_v'''$, where the function $f_v(D)$ is given by

$$f_v(D) = v_{esc}^{-3\mu}\left[1 + \sin(2\gamma)\cot\left(\frac{D}{2r_m}\right) - \cos(2\gamma)\right]^{\frac{3\mu}{2}} = v(D,\gamma)^{-3\mu}. \tag{4.12}$$

The derivative of f_v with respect to D can then be computed as

$$f_v'(D) = \frac{df_v(D)}{dD} = -v_{esc}^{-3\mu}\frac{3\mu}{4}\frac{\sin(2\gamma)}{\sin^2\left(\frac{D}{2r_m}\right)}\left[1 + \sin(2\gamma)\cot\left(\frac{D}{2r_m}\right) - \cos(2\gamma)\right]^{\frac{3\mu}{2}-1}. \tag{4.13}$$

The total mass per ROI area per time for a given ejecta zenith angle γ can be computed by integrating over the sphere of the Moon

$$M_{ROI}(\gamma) = \frac{M_p(1) r_m}{\Delta D^2}\int_{D_{min}}^{D_{max}}\int_0^{2\pi} d\phi dD \sin(D/r_m)\mathcal{V}(D,\gamma)\Phi(D), \tag{4.14}$$

where $\Phi(D)$ is the fraction of azimuth field-of-view (FOV) $\Delta\beta$ from the primary impact location to the ROI location (approximated as a circle[11] of radius $\Delta D/2$). Using Napier's law for spherical triangles, the half-angle azimuth FOV can be computed by

$$\tan(\Delta\beta/2) = \frac{\tan\left(\frac{\Delta D}{2r_m}\right)}{\sin\left(\frac{D+\Delta D/2}{r_m}\right)}, \tag{4.15}$$

[9] By first imposing to integrate over the speed as a function of distance, we give up the ability to study the contribution of ejecta as a function of speed. In order to do this, we must integrate first over the zenith angle space so that we have the remaining terms as a function of distance and speed.

[10] The ΔD^2 terms cancel out.

[11] Although, the area of the ROI is approximated as a rectangle of area ΔD^2.

such that the fraction of FOV is

$$\Phi(D) = \frac{\Delta\beta}{2\pi} = \frac{1}{\pi}\arctan\left[\frac{\tan\left(\frac{\Delta D}{2r_m}\right)}{\sin\left(\frac{D+\Delta D/2}{r_m}\right)}\right]. \tag{4.16}$$

In the limit as $\Delta D \to 0$, we can approximate Equation (4.16) as[12]

$$\Phi(D) \sim \frac{\Delta D}{2\pi r_m \sin(D/r_m)}. \tag{4.17}$$

Therefore, we can see that the $\sin(D/r_m)$ and ΔD terms cancel in Equation (4.14) (which is remarkable! or was it obvious?), so that Equation (4.14) can be simplified to

$$M_{ROI}(\gamma) \sim M_p(1)\left[v(D_{min},\gamma)^{-3\mu} - v(D_{max},\gamma)^{-3\mu}\right], \tag{4.18}$$

$$\sim M_p(> v(D_{min},\gamma)) - M_p(> v(D_{max},\gamma)), \tag{4.19}$$

for $\Delta D \ll r_m$, which is in units of mass per ROI area per time. Equation (4.19) is very interesting, because it tells us that we can directly relate the total ejected mass flux at a particular primary impact location to the total secondary mass flux at the ROI, for a given secondary ejecta angle, in the limit as our ROI length scale is small compared to the radius of the Moon. If we were to introduce a zenith ejecta angle distribution, more work would be needed.

Another remark to make, if we study the simplified integrand of Equation (4.14)*, we can see that the contribution of secondary ejecta as a function of distance and ejecta zenith angle is simply given by* $f_v(D,\gamma) = df_v(D,\gamma)/dD$ *times a* $\sin\gamma$ *term. When studying small angles as the limit as* $\Delta D \to 0$*, one must let* $\gamma = \Delta D/8r_m$*, which will give a finite limit.*

4.2.1 Isotropic Azimuth and $45°$ Zenith Distributions

If we assume that all the ejecta is at $45°$ isotropically and we are interested in ejecta of speeds greater than v_{min}, then the total secondary ejecta mass flux (from Equation (4.19)) at a ROI is given by

$$M_{ROI}(45°) = M_p(> v_{min}) - M_p(> v_{esc}). \tag{4.20}$$

4.2.2 Isotropic Azimuth and Zenith Distributions

In this section, we will assume both an isotropic ejecta distribution in both azimuth and zenith angle. It is not at all obvious from the start, but it turns out that the leading term to the solution to this problem is exactly that of Equation (4.20).

Superficially, the total secondary ejecta mass flux for an isotropic zenith angle distribution is given by

$$M_{ROI,\text{isotropic}} = \frac{\int_{\gamma_{min}}^{\pi/2} d\gamma \sin\gamma M_{ROI}(\gamma)}{\int_{\gamma_{min}}^{\pi/2} d\gamma \sin\gamma}, \tag{4.21}$$

[12] In this case, Mathematica is our friend.

where $M_{ROI}(\gamma)$ is given in Equation (4.18). However, we need to break this integral into separate regions. In all, we need three regions defined in the speed-angle space (see Figure 12 for an example):

Region I: $\gamma_{min} = \gamma^{+}(v_{esc}, \Delta D/2)$, $\gamma_{max} = \gamma^{+}(v_{min}, \Delta D/2)$

Region II: $\gamma_{min} = \gamma^{+}(v_{min}, \Delta D/2)$, $\gamma_{max} = \gamma^{-}(v_{min}, \Delta D/2)$

Region III: $\gamma_{min} = \gamma^{-}(v_{min}, \Delta D/2)$, $\gamma_{max} = \pi/2$

Minimum and Maximum Zenith Angles: First, we will define the minimum and maximum zenith angles for each region.

In region I, γ_{min} can be solved exactly and is given by (see Equation (2.109))

$$\gamma_{I,min} = \gamma^{+}(v_{esc}, \Delta D/2) = \frac{\Delta D}{8r_m}. \tag{4.22}$$

The maximum angle γ_{max} can be approximated by expanding Equation (2.111) for small $D \to \Delta D/2$, such that

$$\gamma_{I,max} = \gamma^{+}(v_{min}, \Delta D/2) \sim \frac{\Delta D}{8r_m}\left(\frac{v_{esc}}{v_{min}}\right)^2 + \mathcal{O}\left(\frac{(\Delta D/r_m)^3}{(v_{min}/v_{esc})^6}\right), \tag{4.23}$$

for $\Delta D/r_m \ll 1$.

In region II, the minimum angle is the same as the maximum angle of the previous section, i.e.

$$\gamma_{II,min} = \gamma_{I,max}. \tag{4.24}$$

The maximum angle γ_{max} is computed by again taking Equation (2.111) and expanding in small $D \to \Delta D/2$ so that we have

$$\gamma_{II,max} = \gamma^{-}(v_{min}, \Delta D/2) \tag{4.25}$$

$$\sim \frac{\pi}{2} - \frac{\Delta D}{8r_m}\left(\frac{v_{esc}}{v_{min}}\right)^2\left[1 - 2\left(\frac{v_{min}}{v_{max}}\right)^2\right] + \mathcal{O}\left(\frac{(\Delta D/r_m)^3}{(v_{min}/v_{esc})^6}\right), \tag{4.26}$$

for $\Delta D/r_m \ll 1$.

Finally, for region III, again we have the same minimum angle as the previous maximum,

$$\gamma_{III,min} = \gamma_{II,max}. \tag{4.27}$$

The maximum angle γ_{max} is simply

$$\gamma_{II,max} = \pi/2. \tag{4.28}$$

We can already notice that in the limit as $\Delta D \to 0$, we expect the integrals in regions I and III to vanish and that the integral in region II will span zenith angles γ from 0 to $\pi/2$, with the limiting speeds as v_{min} and v_{max}.

Integration of Isotropic Zenith Angle Distribution: We begin by breaking up the numerator of Equation (4.21) into the respective regions, so that we have

$$\int_{\gamma_{min}}^{\pi/2} d\gamma \sin\gamma M_{ROI}(\gamma) = \int_{\gamma^+_{(v_{esc},\Delta D/2)}}^{\gamma^+_{(v_{min},\Delta D/2)}} d\gamma \sin\gamma v(\Delta D/2,\gamma)^{-3\mu} \tag{4.29}$$
$$+ \int_{\gamma^+_{(v_{min},\Delta D/2)}}^{\gamma^-_{(v_{min},\Delta D/2)}} d\gamma \sin\gamma v_{min}^{-3\mu}$$
$$+ \int_{\gamma^-_{(v_{min},\Delta D/2)}}^{\pi/2} d\gamma \sin\gamma v(\Delta D/2,\gamma)^{-3\mu}$$
$$- \int_{\gamma^+_{(v_{esc},\Delta D/2)}}^{\pi/2} d\gamma \sin\gamma v_{esc}^{-3\mu}$$

Taking the function $v(\Delta D/2,\gamma)^{-3\mu}$, as defined in Equation (2.110), and taking the limit as $\Delta D \to 0$ we have

$$v(\Delta D/2,\gamma)^{-3\mu} \sim v_{esc}^{-3\mu}\left(\frac{\sin(2\gamma)}{\sin\left(\frac{\Delta D}{4r_m}\right)}\right)^{3\mu/2}\left[1+\mathcal{O}\left(\sin\left(\frac{\Delta D}{4r_m}\right)\frac{1-\cos(2\gamma)}{\sin(2\gamma)}\right)\right], \tag{4.30}$$

as $\Delta D \to 0$. We decided to actually expand in terms of $\sin(x)$ instead of x, for $x = \Delta D/4r_m$. Now we need to further expand Equation (4.30) as $\gamma \to 0$ and $\gamma \to \pi/2$.

For the first limit, we have

$$\sin\gamma v(\Delta D/2,\gamma)^{-3\mu} \sim v_{esc}^{-3\mu}\gamma\left(\frac{8\gamma r_m}{\Delta D}\right)^{3\mu/2}\left[1+\mathcal{O}(\gamma^2,\gamma\Delta D,\Delta D^2)\right], \tag{4.31}$$

as $\Delta D \to 0$ and $\gamma \to 0$.

For the second limit, we have

$$\sin\gamma v(\Delta D/2,\gamma)^{-3\mu} \sim v_{esc}^{-3\mu}\left(\frac{8\gamma' r_m}{\Delta D}\right)^{3\mu/2}\left[\left(1+\frac{\Delta D}{4\gamma' r_m}\right)^{3\mu/2}+\mathcal{O}(\gamma^2,\gamma\Delta D,\Delta D^2)\right], \tag{4.32}$$

as $\Delta D \to 0$ and $\gamma' \to 0$, where $\gamma = \pi/2 - \gamma'$.

The first integral in region I can then be shown to be

$$\int_{\gamma^+_{(v_{esc},\Delta D/2)}}^{\gamma^+_{(v_{min},\Delta D/2)}} d\gamma \sin\gamma v(\Delta D/2,\gamma)^{-3\mu} \sim v_{esc}^{-3\mu}\int_{\frac{\Delta D}{8r_m}}^{\frac{\Delta D}{8r_m}\left(\frac{v_{esc}}{v_{min}}\right)^2} d\gamma\gamma\left(\frac{8\gamma r_m}{\Delta D}\right)^{3\mu/2}, \tag{4.33}$$

$$\sim v_{esc}^{-3\mu}\frac{\left(\frac{v_{esc}}{v_{min}}\right)^{3\mu+4}-1}{32(3\mu+4)}\frac{\Delta D}{r_m}, \tag{4.34}$$

as $\Delta D \to 0$.

In region II, our integral is much easier to evaluate, and is given by

$$\int_{\gamma^+_{(v_{min},\Delta D/2)}}^{\gamma^-_{(v_{min},\Delta D/2)}} d\gamma \sin\gamma v_{min}^{-3\mu} \sim v_{min}^{-3\mu} \int_{\frac{\Delta D}{8r_m}\left(\frac{v_{esc}}{v_{min}}\right)^2}^{\pi/2-\frac{\Delta D}{8r_m}\left(\frac{v_{esc}}{v_{min}}\right)^2\left[1-2\left(\frac{v_{min}}{v_{esc}}\right)^2\right]} d\gamma \sin\gamma, \tag{4.35}$$

$$\sim v_{min}^{-3\mu}\left[1+\frac{1}{8}\left(2-\frac{v_{esc}^2}{v_{min}^2}\right)\frac{\Delta D}{r_m}+\mathcal{O}(\Delta D^2 v_{esc}^4/v_{min}^4)\right], \tag{4.36}$$

as $\Delta D \to 0$.

The next integral in region III, is similar to that of region I. We find that the integral is given by

$$\int_{\gamma^-_{(v_{min},\Delta D/2)}}^{\pi/2} d\gamma \sin\gamma v(\Delta D/2,\gamma)^{-3\mu}, \tag{4.37}$$

$$\sim v_{esc}^{-3\mu}\int_{\pi/2-\frac{\Delta D}{8r_m}\left(\frac{v_{esc}}{v_{min}}\right)^2\left[1-2\left(\frac{v_{min}}{v_{esc}}\right)^2\right]}^{\pi/2} d\gamma\left(2+\frac{8(\pi/2-\gamma)}{\Delta D/r_m}\right)^{3\mu/2}, \tag{4.38}$$

$$\sim v_{esc}^{-3\mu}\frac{\left(\frac{v_{esc}}{v_{min}}\right)^{3\mu+2}-2^{3\mu/2+1}}{4(3\mu+2)}\frac{\Delta D}{r_m}, \tag{4.39}$$

as $\Delta D \to 0$.

Finally, the last integral that spans all regions is like the integral in region II and only requires a simple integral over $\sin$. Therefore, we have

$$\int_{\gamma^+_{(v_{esc},\Delta D/2)}}^{\pi/2} d\gamma \sin\gamma v_{esc}^{-3\mu} \sim v_{esc}^{-3\mu}\int_{\frac{\Delta D}{8r_m}}^{\pi/2} d\gamma\sin\gamma, \tag{4.40}$$

$$\sim v_{esc}^{-3\mu}\left(1-\frac{\Delta D^2}{128r_m^2}+\mathcal{O}(\Delta D^4)\right), \tag{4.41}$$

as $\Delta D \to 0$.

Putting everything together, to first order in ΔD, we finally have

$$\begin{aligned} M_{ROI,\text{isotropic}} \sim\ & v_{min}^{-3\mu}\left[1+\frac{1}{8}\left(2-\frac{v_{esc}^2}{v_{min}^2}\right)\frac{\Delta D}{r_m}\right] \\ & - v_{esc}^{-3\mu}\left[1-\left[\frac{\left(\frac{v_{esc}}{v_{min}}\right)^{3\mu+4}-1}{32(3\mu+4)}+\frac{\left(\frac{v_{esc}}{v_{min}}\right)^{3\mu+2}-2^{3\mu/2+1}}{4(3\mu+2)}\right]\frac{\Delta D}{r_m}\right] \\ & + \mathcal{O}(\Delta D^2), \end{aligned} \tag{4.42}$$

as $\Delta D \to 0$. If the ROI length scale ΔD is to be finite, then we require

$$\frac{\Delta D}{r_m}\left(\frac{v_{esc}}{v_{min}}\right)^4 \ll 1, \tag{4.43}$$

in order for Equation (4.42) to stay valid. The driving contribution to the integral is all from region II, since regions I and III disappear as $\Delta D \to 0$. Note that we account for ejecta that travels less than and greater than half the lunar circumference πr_m.

We can now relate the total secondary ejecta mass flux for an isotropic zenith angle distribution to be the same as if the zenith angle distribution has a delta function at $45°$,

$$M_{ROI,\text{isotropic}} \sim M_{ROI}(45°) + \mathcal{O}\left[\frac{\Delta D}{r_m}\left(\frac{v_{esc}}{v_{min}}\right)^4\right]. \quad (4.44)$$

4.3 Secondary Ejecta at a ROI vs. Distance

We are also interested in studying the contribution of secondary ejecta as a function of distance from the ROI. Instead of integrating over the distances and then integrate over the ejecta angles, we will first integrate over the ejecta zenith angles such that

$$M_{ROI}(D) = -M_p(1)\int_{D/4r_m}^{\pi/2} d\gamma \sin\gamma f_v'(D,\gamma), \quad (4.45)$$

where $f_v'(D,\gamma)$ is given in Equation (4.13). We notice that for all γ in our domain, the integrand is strongly peaked for $D \ll r_m$ and is also dominated by γ near $\pi/4$ or $45°$.

For small D, we can write (using $a = 3\mu/2$)

$$\left[1+\sin(2\gamma)\cot\left(\frac{D}{2r_m}\right) - \cos(2\gamma)\right]^{a-1} \sim \left[\frac{\sin(2\gamma)}{D/2r_m}\right]^{a-1}, \quad (4.46)$$

as $D \to 0$. Therefore, we can write Equation (4.45) as

$$M_{ROI}(D) \sim aM_p(> v_{esc})\int_{D/4r_m}^{\pi/2} d\gamma \frac{\sin\gamma\sin(2\gamma)}{\sin^2\left(\frac{D}{2r_m}\right)}\left[\frac{\sin(2\gamma)}{D/2r_m}\right]^{a-1}, \quad (4.47)$$

as $D \to 0$. Collecting the γ-dependent terms, we let $x = \cos\gamma$ such that $dx = -\sin\gamma d\gamma$,

$$\int_{D/4r_m}^{\pi/2} d\gamma \sin\gamma \sin^a(2\gamma) = 2^a \int_0^{\cos(D/4r_m)} dx x^a (1-x^2)^{a/2}. \quad (4.48)$$

We employ another substitution $y = x^2$ such that $dx = dy/2\sqrt{y}$, giving

$$= 2^{a-1}\int_0^{\cos^2(D/4r_m)} dy y^{\frac{a-1}{2}}(1-y)^{a/2} = 2^{a-1}\beta\left(\cos^2(D/4r_m), \frac{a+1}{2}, \frac{a}{2}+1\right), \quad (4.49)$$

and we notice that this is the integral for the incomplete beta function. Therefore, the contribution of secondary ejecta as a function of distance is given by (replacing $D/4r_m$

by $\tan(D/4r_m)$)

$$M_{ROI}(D) \sim M_p(> v_{esc}) \frac{3\mu}{2} \frac{\cot\left(\frac{D}{4r_m}\right)^{3\mu/2-1}}{\sin^2\left(\frac{D}{2r_m}\right)} \beta\left(\cos^2(D/4r_m), \frac{3\mu+2}{4}, \frac{3\mu}{4}+1\right), \tag{4.50}$$

$$\sim M_p(> v_{esc}) \frac{3\mu}{8} \frac{\Gamma\left(\frac{3\mu+2}{4}\right)\Gamma\left(\frac{3\mu}{4}+1\right)}{\Gamma\left(\frac{3\mu+3}{2}\right)} \left(\frac{D}{4r_m}\right)^{-(3\mu/2+1)}, \tag{4.51}$$

We do note that the normalization factor should not be taken seriously in this calculation. If one then integrates over the entire Moon using Equation (4.51), an overestimate of about a factor of 2.29 will occur. The point is to illustrate that the contribution roughly follows a power law of index $-(3\mu/2+1)$, which for $\mu = 0.4$, the index is -1.6. To compare with the speed distribution $H(v)$, the power law index would be $-(3\mu+1) = -2.2$.

To further expound, we analyzed integrating Equation (4.58) over the speed in order to compute $M_{ROI}(D)$ and we found that the power law index $-(3\mu/2+1)$ on the distance holds for all distances on the Moon. There is a correction term that multiplies the power-law relation that varies at most by 10% over the whole Moon, specifically the pure power-law over estimates the antipodal contributions by a factor of 10, which is insignificant compared to the overall fluxes. Most importantly, the fluxes that originate close to the ROI are correctly modeled by a power-law of the distance.

4.4 Secondary Ejecta at a ROI vs. Speed and Distance

To study the speed distribution as a function of distance, we begin with the speed distribution $H(v)$ and integrate over all contributing angles. For this exercise, we will assume an isotropic distribution. For a given distance and speed, the zenith angle dependence is a multi-valued function for speeds $v/v_{esc} < \sqrt{2}/2$ and a single-valued function for speeds $v/v_{esc} \geqslant \sqrt{2}/2$.

The integral over the secondary ejecta as a function of speed and distance is given by

$$M_{ROI}(D, v) = dA(D)\Phi(D)H(v) \int_{\gamma_{min}}^{\gamma_{max}} d\gamma \sin\gamma. \tag{4.52}$$

We must break up the integral over the zenith angle into two regions in order to have a single-valued function, one less than the optimal angle γ_{opt} and one greater than. In the limit as the ROI size goes to zero, the region between the two cases goes away, so we will not worry about it here. Breaking up the integral, we have (assuming[13] $v > v_{min}$)

$$\int_{\gamma_{min}}^{\gamma_{max}} d\gamma \sin\gamma = \int_{\gamma^+(D_0,v)}^{\gamma^+(D_1,v)} d\gamma \sin\gamma + \begin{cases} \int_{\gamma^-(D_1,v)}^{\gamma^-(D_0,v)} d\gamma \sin\gamma & \text{for } D \leqslant \pi r_m \text{ and } \frac{v^2}{v_{esc}^2} \leqslant \frac{1}{2} \\ 0 & \text{for } D > \pi r_m \text{ or } \frac{v^2}{v_{esc}^2} > \frac{1}{2} \end{cases}, \tag{4.53}$$

[13] The v_{min} defined here is different from previous usage in Section 4.

where $D_0 = D - \Delta D/2$ and $D_1 = D + \Delta D/2$ with the ROI width diameter of ΔD. We also note that the minimum speed v_{min} for a given distance D is given by (see also Equation (2.113))

$$\frac{v_{min}^2}{v_{esc}^2} = \frac{\tan\left(\frac{D}{2r_m}\right)}{\tan\left(\frac{\pi}{4} - \frac{D}{4r_m}\right)}. \tag{4.54}$$

We can also express the maximum distance that can be reached as a function of speed

$$\cot\left(\frac{D_{max}}{2r_m}\right) = \frac{\sqrt{1-2x^2}}{x^2}. \tag{4.55}$$

The angles $\gamma^{\pm}$ are given by (see Equation (2.111))

$$\cot\gamma^{\pm} = x^2\cot\left(\frac{D}{2r_m}\right) \pm \sqrt{x^4\cot^2\left(\frac{D}{2r_m}\right) + (2x^2-1)}. \tag{4.56}$$

The optimal angle in terms of the ejecta speed can also be written as (see also Equation (2.116))

$$\cot\gamma_{opt}^{\pm} = \sqrt{1-2x^2}. \tag{4.57}$$

Evaluating the integrals and letting $\Delta D \to 0$, we arrive at the following solution:

$$M_{ROI}(D,v) \sim dA(D)\Phi(D)H(v)\Delta D\mathcal{G}(D,v), \tag{4.58}$$

where the geometrical term of the secondary ejecta speed distribution is (see Figure 14 for an example)

$$\mathcal{G}(D,v) \sim \begin{cases} -\frac{d}{dD}\cos\gamma^{+} + \frac{d}{dD}\cos\gamma^{-} & \text{for } D \leqslant \pi r_m \text{ and } \frac{v_{min}^2}{v_{esc}^2} \leqslant \frac{v^2}{v_{esc}^2} \leqslant \frac{1}{2} \\ -\frac{d}{dD}\cos\gamma^{+} & \text{for } D > \pi r_m \text{ or } \frac{v^2}{v_{esc}^2} > \frac{1}{2} \\ 0 & \text{for } \frac{v^2}{v_{esc}^2} < \frac{v_{min}^2}{v_{esc}^2}, \end{cases} \tag{4.59}$$

for $\Delta D \to 0$ and the $\cos\gamma^{\pm}$ terms can be computed from the $\cot\gamma^{\pm}$ equation by

$$\cos\gamma^{\pm} = \frac{\cot\gamma^{\pm}}{\sqrt{1+\cot^2\gamma^{\pm}}}. \tag{4.60}$$

In Figure 14, we can see that for distances less than πr_m, i.e. less than half the lunar circumference, the speed distribution decreases for larger speeds. However, for distances greater than half the lunar circumference, only speeds $v > \frac{\sqrt{2}}{2}v_{esc}$ are valid and the speed distribution increases for larger speeds. The fastest speeds near the escape speed seem to be more prevalent from distances $D > \pi r_m$. It is also evident that the ejecta originating from close distances dominates the total secondary ejecta.

Not shown in Figure 14 due to plotting artifacts and scaling, the peaks as a function of speed are proportional to $\propto v^{-2}$ for speeds $v < \frac{\sqrt{2}}{2}v_{esc}$

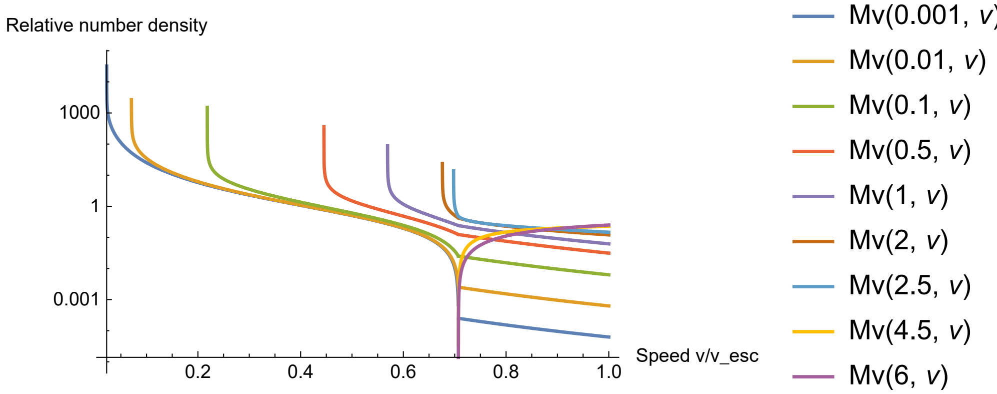

Figure 14: The geometrical term of the secondary ejecta speed distribution $\mathcal{G}(D, v)$ as a function of speed for various distances in units of lunar radii r_m.

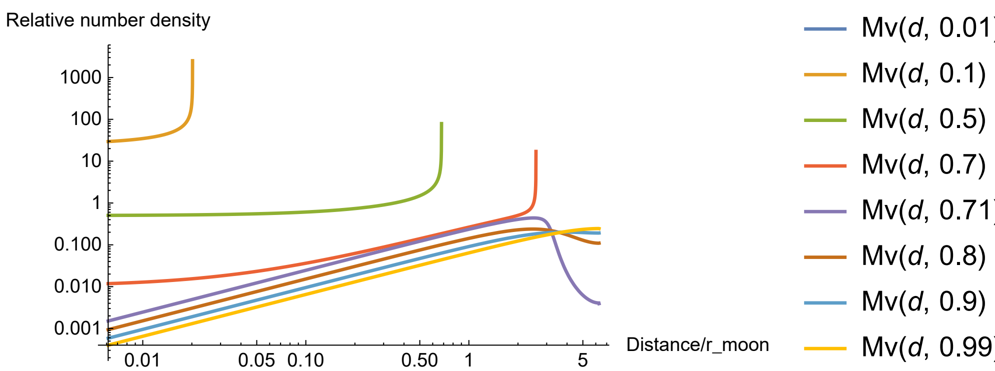

Figure 15: The geometrical term of the secondary ejecta distance distribution $\mathcal{G}(D, v)$ as a function of distance, in units of lunar radii r_m, for various speeds in units of escape velocity v_{esc}.

Ejecta distance distribution: We can also study the distance distribution as a function of speed. This shows where the majority of the contribution is at a certain distance for a particular ejecta speed.

In Figure 15, we see that for ejecta speeds $x < \sqrt{2}/2 \approx 0.7071$, the main contribution of ejecta comes from very particular distances (i.e., a ring of distances centered on the ROI). For speeds in the range $\sqrt{2}/2 < x < 0.9$, there is an approximate range of distances $0.35 < D/2r_m < 0.6$ that contribute to the ejecta flux (i.e., a hemispherical cap centered on the antipode location). And finally, for speeds $0.9 < x < 1$, the contribution of distances to the ejecta flux are $0.4 < D/2r_m < 1$ (i.e., the entire surface of the Moon contributes to this speed range).

To summarize, the contribution of ejecta for a particular speed ($x = v/v_{esc}$) originates from:

- Slowest speeds ($x < \sqrt{2}/2 \approx 0.7071$): ring of locations centered on the ROI,
- Intermediate speeds ($\sqrt{2}/2 < x < 0.9$): hemispherical cap of locations centered on the antipode,
- Fast speeds ($0.9 < x < 1$): the entire surface of the Moon.

If we include the fact that the speed distribution follows a power-law, then we can conclude that most of the ejecta comes from nearby (fraction of the Moon's radius) at slow speeds (less than $0.7 \times v_{esc}$). However, in terms of penetration risk, there may be other speeds and hence a larger portion of the Moon that contribute to our problem.

4.5 Secondary Ejecta at a Satellite of the Moon

In this section, we will derive more general equations than what was done in Section 2.11 by assuming the final impact radius to be different from the ejected radius, where before we assumed the heights were the same. For convenience, we rewrite Equations (2.98), (2.99), and (2.100) here:

$$\frac{a}{r_m} = \frac{1}{2\left(1 - \frac{v^2}{v_{esc}^2}\right)}, \tag{4.61}$$

where $r_m = 1737.1$ km is the radius of the Moon and $v_{esc} = 2.38$ km/s is the Moon's escape velocity, and

$$e = \sqrt{\left(\frac{2v^2}{v_{esc}^2} - 1\right)^2 \sin^2\gamma + \cos^2\gamma}, \tag{4.62}$$

where we employed the fact that the gravity of the Moon is $g = GM/r_m^2$ and the escape velocity is related by $v_{esc} = \sqrt{2gr_m}$. The third equation we need gives the location in the elliptical orbit by the angle β from the perilune, the semi-major axis a, and the eccentricity e by

$$r = \frac{a(1-e^2)}{1 + e\cos\beta}. \tag{4.63}$$

We will define the p-subscripts by the particle ejecta location and the s-subscripts by the satellite location. Unless stated otherwise, we will assume the ejecta speed v_p and zenith angle γ_p are given in addition to the satellite radius r_s from the center of the Moon.

Satellite Angle from Periapsis The satellite location with respect to the perilune β_s has a similar structure to that of the location of the ejecta β_p, given by

$$\tan\beta_s = \frac{2\frac{v_p^2}{v_{esc}^2}\sin\gamma_p\cos\gamma_p}{2\frac{r_m}{r_s}\frac{v_p^2}{v_{esc}^2}\sin^2\gamma_p - 1} F_s(r_s, v_p, \gamma_p), \tag{4.64}$$

where the factor F_s is given by

$$F_s(r_s, v_p, \gamma_p) = \sqrt{1 + \frac{1 - \frac{r_m}{r_s}}{\cos^2\gamma_p}\left[\sin^2\gamma_p\left(1 + \frac{r_m}{r_s}\right) - \frac{v_{esc}^2}{v_p^2}\right]}. \tag{4.65}$$

Ejecta Local Zenith Angle at Satellite The local zenith angle of the ejecta at the satellite γ_s starts from

$$\tan\left(\frac{\pi}{2} - \gamma_s\right) = \frac{e \sin\beta_s}{1 + e\cos\beta_s}, \tag{4.66}$$

where

$$e\cos\beta_s = \frac{a}{r_s}(1 - e^2) - 1 \tag{4.67}$$

$$= 2\frac{r_m}{r_s}\frac{v_p^2}{v_{esc}^2}\sin^2\gamma_p - 1, \tag{4.68}$$

$$e\sin\beta_s = \sqrt{e^2 - (e\cos\beta_s)^2} \tag{4.69}$$

$$= 2\frac{v_p^2}{v_{esc}^2}\sin\gamma_p\cos\gamma_p F_s(r_s, v_p, \gamma_p), \tag{4.70}$$

such that

$$\cot\gamma_s = \frac{r_s}{r_m}\cot\gamma_p F_s(r_s, v_p, \gamma_p). \tag{4.71}$$

Maximum Apoapsis of Ejecta The maximum height r_{max} (i.e., the apoapsis) the ejecta of speed v_p and zenith angle γ_p is given by (fixing the typo in Equation 16 of *Gault et al.* [1963])

$$\frac{r_{\text{max}}}{r_m} = \frac{1 + \sqrt{1 - 4\frac{v_p^2}{v_{esc}^2}\left(1 - \frac{v_p^2}{v_{esc}^2}\right)\sin^2\gamma_p}}{2\left(1 - \frac{v_p^2}{v_{esc}^2}\right)} \tag{4.72}$$

Restriction of Ejecta Speed for known Satellite Height and Ejecta Angle To reach a particular satellite radius $r_s = r_{\text{max}}$ for a given ejecta angle γ_p, we have the following condition on the ejecta speed v_p:

$$\frac{v_p}{v_{esc}} = \sqrt{\frac{\frac{r_{\text{max}}}{r_m}\left(\frac{r_{\text{max}}}{r_m} - 1\right)}{\frac{r_{\text{max}}^2}{r_m^2} - \sin^2\gamma_p}}. \tag{4.73}$$

To find the speed of the ejecta at the satellite height, use the following expression.

Ejecta Speed at Satellite The speed of the ejecta at the satellite orbital radius given the initial ejecta speed is given by

$$\frac{v_s}{v_{esc}} = \sqrt{\frac{r_m}{r_s} + \frac{v_p^2}{v_{esc}^2} - 1}. \tag{4.74}$$

If $r_s \to \infty$, then v_∞ is the hyperbolic excess speed

$$\frac{v_\infty}{v_{esc}} = \sqrt{\frac{v_p^2}{v_{esc}^2} - 1}. \tag{4.75}$$

Rearranging to solve for the ejecta speed v_p, we have

$$\frac{v_p}{v_{esc}} = \sqrt{1 - \frac{r_m}{r_s} + \frac{v_s^2}{v_{esc}^2}}. \tag{4.76}$$

Geographic Distance between Impact Point and Satellite The geographic distance between the point of primary impact and the satellite D_s can be related between the difference between angles from periapsis

$$\frac{D_s}{r_m} = \beta_s - \beta_p. \tag{4.77}$$

Taking the tangent of this difference, we can use Equations (4.64) and (2.107) for the satellite and point-of-impact (POI) periapsis angles β_s and β_p such that

$$\begin{aligned} \tan\left(\frac{D_s}{r_m}\right) &= \tan(\beta_s - \beta_p) \\ &= \frac{\tan\beta_s - \tan\beta_p}{1 + \tan\beta_s \tan\beta_p} \end{aligned} \tag{4.78}$$

In terms of the satellite angle from periapsis β_s, we have

$$\tan\beta_s = \frac{\tan(D_s/r_m) + \tan\beta_p}{1 - \tan(D_s/r_m)\tan\beta_p}. \tag{4.79}$$

We could then assume a specific location of the satellite defined by it's height and geographic distance from the POI and find the valid ejecta angles and speeds.

References

Bjorkman, M. D., and E. L. Christiansen, An astronaut's risk of experiencing a critical impact from lunar ejecta during lunar eva, *First Int'l. Orbital Debris Conf.*, 2019.

Bouley, S., et al., Power and duration of impact flashes on the moon: Implication for the cause of radiation, *Icarus*, *218*(1), 115–124, 2012.

Brown, P., R. Spalding, D. O. ReVelle, E. Tagliaferri, and S. Worden, The flux of small near-earth objects colliding with the earth, *Nature*, *420*(6913), 294, 2002.

Carrier, W. D., Lunar soil grain size distribution, *The moon*, *6*(3-4), 250–263, 1973.

Carrier III, W. D., Particle size distribution of lunar soil, *Journal of Geotechnical and Geoenvironmental Engineering*, *129*(10), 956–959, 2003.

Cour-Palais, B. G., Meteoroid environment model 1969 (near earth to lunar surface), nasa sp-8013, *National Aeronautics and Space Administration, Washington, DC*, 1969.

Gault, D. E., Impact cratering, in *A primer in lunar geology*, 1974.

Gault, D. E., and J. A. Wedekind, Experimental studies of oblique impact, in *Lunar and Planetary Science Conference Proceedings*, vol. 9, pp. 3843–3875, 1978.

Gault, D. E., E. M. Shoemaker, and H. J. Moore, *NASA TN D-1767 Spray ejected from the lunar surface by meteoroid impact*, National Aeronautics and Space Administration, 1963.

Grün, E., H. Zook, H. Fechtig, and R. Giese, Collisional balance of the meteoritic complex, *Icarus*, *62*(2), 244–272, 1985.

Holsapple, K., The scaling of impact processes in planetary sciences, *Annual review of earth and planetary sciences*, *21*(1), 333–373, 1993.

Horányi, M., J. Szalay, S. Kempf, J. Schmidt, E. Grün, R. Srama, and Z. Sternovsky, A permanent, asymmetric dust cloud around the moon, *Nature*, *522*(7556), 324–326, 2015.

Horányi, M., et al., The lunar dust experiment (ldex) onboard the lunar atmosphere and dust environment explorer (ladee) mission, *Space Science Reviews*, *185*(1-4), 93–113, 2014.

Housen, K. R., and K. A. Holsapple, Ejecta from impact craters, *Icarus*, *211*(1), 856–875, 2011.

Koschny, D., and E. Grün, Impacts into ice–silicate mixtures: Crater morphologies, volumes, depth-to-diameter ratios, and yield, *Icarus*, *154*(2), 391–401, 2001.

Krivov, A. V., M. Sremčević, F. Spahn, V. V. Dikarev, and K. V. Kholshevnikov, Impact-generated dust clouds around planetary satellites: spherically symmetric case, *Planetary and Space Science*, *51*(3), 251–269, 2003.

Miller, A., Esabase2 debris release 10.0 technical description, *Tech. Rep. 1.7*, ESA, 2017.

Moore, H., D. Gault, and R. Lugn, Experimental impact craters in basalt, *Trans. Min. Eng*, *229*, 258–262, 1963.

Moorhead, A. V., A. Kingery, and S. Ehlert, Nasa's meteoroid engineering model 3 and its ability to replicate spacecraft impact rates, *Journal of Spacecraft and Rockets*, pp. 1–17, 2019.

Moser, D., R. Suggs, W. Swift, R. Suggs, W. Cooke, A. Diekmann, and H. Koehler, Luminous efficiency of hypervelocity meteoroid impacts on the moon derived from the 2006 geminids, 2007 lyrids, and 2008 taurids, *Meteoroids: The Smallest Solar System Bodies*, p. 142, 2011.

Moser, D., R. Suggs, and R. Suggs, Large meteoroid impact on the moon on 17 march 2013, in *Asteroids, Comets, Meteors 2014*, 2014.

Neukum, G., B. A. Ivanov, and W. K. Hartmann, Cratering records in the inner solar system in relation to the lunar reference system, in *Chronology and evolution of Mars*, pp. 55–86, Springer, 2001.

Rival, M., and J. Mandeville, Modeling of ejecta produced upon hypervelocity impacts, *Space debris*, *1*(1), 45–57, 1999.

Robinson, M. S., et al., New crater on the moon and a swarm of secondaries, *Icarus*, *252*, 229–235, 2015.

Shuvalov, V., Ejecta deposition after oblique impacts: An influence of impact scale, *Meteoritics & Planetary Science*, *46*(11), 1713–1718, 2011.

Vickery, A., Size-velocity distribution of large ejecta fragments, *Icarus*, *67*(2), 224–236, 1986.

Zook, H. A., The problem of secondary ejecta near the lunar surface., in *Transactions of the 1967 National Symposium on Saturn V/Apollo and Beyond*, vol. I, pp. EN–8, 1967.